Topics in Mining, Metallurgy and Materials Engineering
*Series Editor:* Carlos P. Bergmann

Marcel Antonio Arcari Bassani
João Felipe Coimbra Leite Costa

# Geostatistics with Data of Different Support Applied to Mining Engineering

Springer

# Topics in Mining, Metallurgy and Materials Engineering

"Topics in Mining, Metallurgy and Materials Engineering" welcomes manuscripts in these three main focus areas: Extractive Metallurgy/Mineral Technology; Manufacturing Processes, and Materials Science and Technology. Manuscripts should present scientific solutions for technological problems. The three focus areas have a vertically lined multidisciplinarity, starting from mineral assets, their extraction and processing, their transformation into materials useful for the society, and their interaction with the environment.

**** Indexed by Scopus (2020) ****

More information about this series at http://www.springer.com/series/11054

Marcel Antonio Arcari Bassani ·
João Felipe Coimbra Leite Costa

# Geostatistics with Data of Different Support Applied to Mining Engineering

Springer

Marcel Antonio Arcari Bassani
Mineral Exploration and Mining Planning Laboratory—LPM
Department of Mining Engineering
Federal University of Rio Grande do Sul
Porto Alegre, Rio Grande do Sul, Brazil

João Felipe Coimbra Leite Costa
Mineral Exploration and Mining Planning Laboratory—LPM
Department of Mining Engineering
Federal University of Rio Grande do Sul
Porto Alegre, Rio Grande do Sul, Brazil

ISSN 2364-3293 ISSN 2364-3307 (electronic)
Topics in Mining, Metallurgy and Materials Engineering
ISBN 978-3-030-80192-2 ISBN 978-3-030-80193-9 (eBook)
https://doi.org/10.1007/978-3-030-80193-9



This Springer imprint is published by the registered company Springer Nature Switzerland AG
The registered company address is: Gewerbestrasse 11, 6330 Cham, Switzerland

*Marcel Antonio Arcari Bassani dedicates the book to his beloved wife Waleska.*

*João Felipe Coimbra Leite Costa dedicates to Luciana and Juan, his precious jewels.*

# Preface

This book aims to bring some new insights in using data of different support for mining applications. The integration of data of different support in Geostatistics is not a novelty in the geostatistical literature. However, most textbooks require a solid mathematical background, which is sometimes a barrier for many readers. In addition, many case studies about this topic shown in journal papers and conference proceedings are related to petroleum and remote sensing areas. In this book, we tried to keep the theory minimum and focus on case studies relevant to Mining Engineering.

The book is appropriate for professional engineers and geologists who work in the area of mineral resource estimation. Moreover, we believe most graduate and undergraduate students who have recently started studying Geostatistics will significantly benefit from the content presented.

The book is organized in eight chapters as follows:

- Chapter 1 provides an introduction to the topic of data of different support and reviews previous works;
- Chapter 2 discusses solutions to integrate data of different support into Geostatistics using kriging;
- Chapter 3 details the methods to perform geostatistical simulations with data of different support;
- Chapter 4 presents the change of support using the variogram for variogram regularization and deconvolution;
- Chapter 5 illustrates the solution of integrating data of different support in kriging in a case study;
- Chapter 6 presents a case study applied to continuous variables using Direct Sequential Simulation with data of different support;
- Chapter 7 is a case study of sequential indicator simulation with categorical data of different support;
- Chapter 8 closes with some conclusions.

The research presented in this book was developed in the Mineral Exploration and Mining Planning Laboratory (LPM) of the Federal University of Rio Grande do Sul (UFRGS). In this regard, the authors are grateful to all the LPM students and industry

affiliates. Moreover, the LPM has benefited from extensive interaction with other geostatistical centers, such as those from the Stanford University, University of Alberta (UofA), and Instituto Superior Técnico (IST). Remarkably, the authors acknowledge the positive influence that Professors Clayton Deutsch (UofA), Jef Caers (Stanford), Alexandre Boucher (AR2Tech), Amílcar Soares (IST), and Leonardo Azevedo (IST) had on the LPM research group. In summary, all the people who have frequented the LPM made the laboratory a thriving research environment.

Porto Alegre, Brazil

Marcel Antonio Arcari Bassani
João Felipe Coimbra Leite Costa

# Contents

# Abbreviations

| | |
|---|---|
| BSSIM | Block Sequential Simulation |
| ccdf | Conditional cumulative distribution function |
| cdf | Cumulative distribution function |
| DDH | Diamond drill holes |
| DSS | Direct Sequential Simulation |
| LHS | Left-hand-side |
| LMC | Linear Model of Coregionalization |
| REC14 | Proportion of mass retained at 14 # sieve aperture |
| RHS | Right-hand-side |
| SGS | Sequential Gaussian Simulation |
| SIS | Sequential Indicator Simulation |
| SMU | Selective mining unity |
| TBS | Turning Bands Simulation |

# Chapter 1
# Introduction


## 1.1 Data of Different Support

Geostatistical techniques are extensively used for mineral resources assessment, including grade estimation and uncertainty analysis. Support is the term used in Geostatistics to describe the size or volume of a sample. For example, suppose a grade sample obtained from diamond drill holes (DDH). In this case, the support is a function of the core's radius and length.

In Mining Engineering applications, data that have different support are often found. For instance, many mining operations contain datasets collected in different years, with different sampling protocols and core lengths. Another example is production data, including averaged grades over a mined out area. When the data have different support, this difference should be considered to build grade models.

The use of data of different support is well established in the petroleum industry. The petroleum industry routinely combines information from wells and seismic surveys. The wells have a vertical resolution of decimeters, whereas the seismic data have a vertical resolution of ten meters or more (Pyrcz and Deutsch 2014). The seismic data usually consist of a coarse grid where all the grid cells have the same size. Moreover, the seismic data often cover the entire area of interest.

This scenario rarely occurs in Mining Engineering applications. The data of different support are usually scattered in the area of interest. Moreover, the samples usually have different sizes. For instance, consider a dataset with data obtained from ten different sampling campaigns that used distinct sampling protocols. The samples are scattered over the area of interest and probably have different lengths.

One alternative to deal with samples of different lengths is to transform the original 3D dataset into a 2D dataset and work with the variable accumulation (Journel and Huijbregts 1978; Krige 1981; Bertoli et al. 2003; Marques et al. 2014). Accumulation is the product of grade and thickness. The problem is that this approach disregards the vertical mining selectivity.

Another alternative consists of compositing the samples and estimate using the composites (Rossi and Deutsch 2014). Compositing involves combining adjacent



M. A. Arcari Bassani and J. F. Coimbra Leite Costa, *Geostatistics with Data of Different Support Applied to Mining Engineering*, Topics in Mining, Metallurgy and Materials Engineering, https://doi.org/10.1007/978-3-030-80193-9_1

samples along one drill hole and calculating their average according to a specific length. However, compositing is a challenge when the length of the samples is highly variable. Compositing to a long length smooths the original grades, which may mask important short-scale geological structures. In contrast, compositing to a short length usually breaks the initial sample into several pieces with the same grade. The latter leads to an incorrect result and artificially diminishes the short-scale variability.

## 1.2 Previous Works

Many geostatistical books (Journel and Huijbregts 1978; Isaaks and Srivastava 1989; Goovaerts 1997) show how the kriging system may accommodate data of different support. In simple terms, the relationship between the data in kriging is obtained by covariances. The data representing a volume in the space are defined as "block data" (even though the block may have any shape), while the data representing a point in the space are called point data. The relationships between these two types of data are defined in the kriging system by point-to-block and block-to-block covariances.

The point-to-block covariances are primarily used for the block kriging algorithm (Journel and Huijbregts 1978; Isaaks and Srivastava 1989; Goovaerts 1997). Block kriging consists of estimating the average value of a volume using point samples. The kriging system is modified, so that the right-hand-side matrix uses point-to-block covariances. The result is that the average grade over a volume is estimated directly with one system of equations. Journel and Huijbregts (1978) proved that the block kriging estimate equals the linear average of point kriging estimates over the block volume. In summary, the point-to-block and block-to-block covariances preserve the linear relationship between the data of different support. Point-to-block and block-to-block covariances are linear average covariances calculated over points that discretize the blocks or volumes of interest.

When the data have different support and precision, Deutsch et al. (1996) affirm that this difference must be considered. In this context, the block cokriging approach is the most rigorous method to integrate these two sources of information. Similar to block kriging, block cokriging also uses average covariances to consider the difference in support between the data.

The main difference between block kriging and cokriging is that block kriging calculates all the covariances using the one variogram model, which refers to the variable of interest. This approach is the proper method when the data differ in support but not in precision. In contrast, the block cokriging approach uses the Linear Model of Coregionalization (MLC—Goovaerts 1997) to calculate the covariances. As a result, the average covariances would be calculated through the cross-variogram model. This book was focused on the difference in support between the samples, so block kriging was mainly used for the case studies.

Behrens et al. (1998) proposed the Sequential Gaussian Simulation (SGS—Isaaks 1990) with block kriging to incorporate the seismic data. The drawback is that the Sequential Gaussian Simulation uses a nonlinear transformation. The result is that

the linear relationship between the data of different support is lost, consequently the block kriging approach with average covariances is inadequate.

Deutsch (2002) recommends avoiding nonlinear transformations when dealing with data of different support. The use of nonlinear transformations is a limitation for the Gaussian simulation algorithms such as Sequential Gaussian Simulation (SGS) and Turning Bands Simulation (TBS—Journel and Huijbregts 1978). These methods transform the original data into Gaussian values. In this context, the Direct Sequential Simulation (DSS—Journel 1994; Soares 2001) stands out as it uses the data directly.

Tran et al. (2001) used DSS with average covariances to integrate data of different support. As DSS does not use nonlinear transformations, the linear relationship between the data of different support is kept. The example shown by the authors combined data from wells, seismic surveys, and production tests. Yao and Journel (2000) also used DSS to build porosity models in an oil reservoir. The seismic information was incorporated by block cokriging.

The DSS that considers data of different support was implemented by Hansen and Mosegaard (2008) in the VISIM software. The software allowed use of volumetric data of irregular shapes for geostatistical simulations. A complete software package to integrate data of different support, called Bgeostats, was published by Liu and Journel (2009). The Bgeostats consisted of a series of plug-ins for SGeMS (Remy et al. 2008) and included algorithms for estimation and simulation.

The use of average covariances to integrate data of different support may also be used for categorical variables. In this context, Yao and Chopra (2000) utilized Sequential Indicator Simulation (SIS) with block cokriging to incorporate the lithology proportion derived from seismic to build simulated lithology models in a reservoir. The use of average covariances for simulation of categorical variables was implemented in the BlockSIS software (Deutsch 2006).

## References

Behrens RA, MacLeod MK, Tran TT, Alimi AC (1998) Incorporating seismic attribute maps in 3D reservoir models. SPE Reservoir Eval Eng 1(02):122–126

Bertoli O, Vann J, Dunham S (2003) Two-dimensional geostatistical methods—theory, practice and a case study from the 1A shoot nickel deposit, Leinster, Western Australia. In: 5th International mining geology conference

Deutsch CV (2002) Geostatistical reservoir modeling. Oxford University Press, New York

Deutsch CV (2006) A sequential indicator simulation program for categorical variables with point and block data: BlockSIS. Comput Geosci 32(10):1669–1681

Deutsch CV, Srinivasan S, Mo Y (1996) Geostatistical reservoir modeling accounting for precision and scale of seismic data. In: SPE annual technical conference and exhibition. Society of Petroleum Engineers. https://doi.org/10.2118/36497-MS

Goovaerts P (1997) Geostatistics for natural resource evaluation. Oxford University Press, Oxford

Hansen TM, Mosegaard K (2008) VISIM: sequential simulation for linear inverse problems. Comput Geosci 34(1):53–76

Isaaks EH (1990) The application of Monte Carlo methods to the analysis of spatially correlated data. PhD Thesis, Stanford University

Isaaks HE, Srivastava MR (1989) An introduction to applied geostatistics. Oxford University Press, Oxford

Journel AG (1994) Modeling uncertainty: some conceptual thoughts. Geostatistics for the next century. Springer, Dordrecht, pp 30–43

Journel AG, Huijbregts CJ (1978) Mining geostatistics. Academic Press, New York

Krige DG, Krige DG (1981) Lognormal-de Wijsian geostatistics for ore evaluation. South African Institute of mining and metallurgy, Johannesburg

Liu Y, Journel AG (2009) A package for geostatistical integration of coarse and fine scale data. Comput Geosci 35(3):527–547

Marques DM, Rubio RH, Costa JFCL, Silva EMAD (2014) The effect of accumulation in 2D estimates in phosphatic ore. REM: Revista Escola de Minas 67(4):431–437

Pyrcz MJ, Deutsch CV (2014) Geostatistical reservoir modeling. Oxford University Press, New York

Remy N, Boucher A, Wu J (2008) Applied geostatistics with SGeMS: a user's guide. Cambridge University Press, New York

Rossi ME, Deutsch CV (2014) Mineral resource estimation. Springer, Berlin

Soares A (2001) Direct sequential simulation and cosimulation. Math Geosci 33(8):911–926

Tran TT, Deutsch CV, Xie Y (2001) Direct geostatistical simulation with multiscale well, seismic, and production data. In: SPE annual technical conference and exhibition. Society of Petroleum Engineers. https://doi.org/10.2118/71323-MS

Yao T, Chopra A (2000) Integration of seismic attribute map into 3D facies modeling. J Petrol Sci Eng 27(1–2):69–84

Yao T, Journel AG (2000) Integrating seismic attribute maps and well logs for porosity modeling in a west Texas carbonate reservoir: addressing the scale and precision problem. J Petrol Sci Eng 28(1–2):65–79

# Chapter 2
# Kriging with Data of Different Support


Support is the term used in the geostatistical literature to describe the volume or size of the data. For instance, the average grade of a mined pushback refers to a volume/support much larger than a sample that represents the average grade along one meter of a diamond drill hole. This difference in support must be considered if these two sources of information are used to build grade models.

This chapter reviews some fundamentals of kriging and details the use of data of different support for geostatistical applications. The use of average covariances to integrate data of different support is highlighted. An illustrative example is provided, and the effects of the data support in the estimates are discussed.

## 2.1 Overview of Kriging

Kriging was established for the problem of estimating a continuous attribute $z$ at location $\mathbf{u}$ using a linear combination of the $n$ surrounding samples $\{z(\mathbf{u}_i), i = 1, \ldots, n\}$. All types of kriging are variants of the general kriging estimator (Eq. 2.1):

$$z^*(\mathbf{u}) - m(\mathbf{u}) = \sum_{i=1}^{n} \lambda_i \cdot [z(\mathbf{u}_i - m(\mathbf{u}_i)], \tag{2.1}$$

where $\lambda_i$ is the weight of the datum $z(\mathbf{u}_i)$. The values $m(\mathbf{u})$ and $m(\mathbf{u}_i)$ are the means of the attribute at locations $\mathbf{u}$ and $\mathbf{u}_i$, respectively. These means are called as trend components. Trends that are known should be treated deterministically and, thus, the weights are applied to the residuals, which are the difference between the attribute considered and its mean. What differs the variants of kriging is the way these trend components are considered.

The mathematical formulation of the kriging equations is well explained in classic geostatistical books (Journel and Huijbregts 1978; Isaaks and Srivastava 1989; Deutsch and Journel 1998; Goovaerts 1997). In this book, we quickly review the



M. A. Arcari Bassani and J. F. Coimbra Leite Costa, *Geostatistics with Data of Different Support Applied to Mining Engineering*, Topics in Mining, Metallurgy and Materials Engineering, https://doi.org/10.1007/978-3-030-80193-9_2

simple and ordinary kriging techniques and emphasize the use of data of different support in Geostatistics. Simple and ordinary kriging are the most used kriging algorithms in the mining industry. Simple kriging is widely used for simulation studies, while ordinary kriging is the main estimation technique for mineral resource estimation.

## 2.2 Simple Kriging

Simple kriging assumes that the mean $m$ is known and constant over the entire area of interest. The simple kriging estimate is a linear combination of the samples and the mean $m$ (Eq. 2.2):

$$\begin{aligned} z^*(\mathbf{u}) &= \sum_{i=1}^{n} \lambda_i \cdot [z(\mathbf{u}_i) - m] + m \\ z^*(\mathbf{u}) &= \sum_{i=1}^{n} \lambda_i \cdot z(\mathbf{u}_i) + \left[1 - \sum_{i=1}^{n} \lambda_i\right] \cdot m, \end{aligned} \tag{2.2}$$

where $z^*(\mathbf{u})$ is the estimate, $\lambda_i$ are the simple kriging weights, and $z(\mathbf{u}_i)$ are the data values.

The simple kriging weights are chosen, so that the error variance is minimized. The error variance is expressed using the random variables $Z^*(\mathbf{u})$ and $Z(\mathbf{u})$, which represent the estimated and true values at location $\mathbf{u}$. A detailed explanation of random variables is provided by Isaaks and Srivastava (1989). Equation 2.3 defines the error variance:

$$\begin{aligned} \sigma_E^2(\mathbf{u}) &= \mathrm{Var}\{\ Z^*(\mathbf{u}) - Z(\mathbf{u})\} \\ \sigma_E^2(\mathbf{u}) &= \mathrm{Var}\{\ Z^*(\mathbf{u})\} - 2\mathrm{Cov}\{Z^*(\mathbf{u}), Z(\mathbf{u})\} + \mathrm{Var}\{Z(\mathbf{u})\}, \end{aligned} \tag{2.3}$$

Considering that the estimate $Z^*(\mathbf{u})$ is a linear combination of the data values (Eq. 2.2), the error variance may be expressed as a function of the estimation weights and covariances (Eq. 2.4):

$$\sigma_E^2(\mathbf{u}) = \sum_{i=1}^{n} \sum_{j=1}^{n} \lambda_i \cdot \lambda_j \cdot C(\mathbf{u}_i, \mathbf{u}_j) - 2 \cdot \sum_{i=1}^{n} \lambda_i \cdot C(\mathbf{u}_i, \mathbf{u}) + C(0), \tag{2.4}$$

where $\lambda_i$ are the estimation weights, $C(\mathbf{u}_i, \mathbf{u}_j)$ is the covariance between the data located at $\mathbf{u}_i$ and $\mathbf{u}_j$, $C(\mathbf{u}_i, \mathbf{u})$ is the covariance between the datum located at $\mathbf{u}_i$ and the point $\mathbf{u}$ to be estimated, and $C(0)$ is the variance of the data. The terms $C(0)$, $C(\mathbf{u}_i, \mathbf{u})$, and $C(\mathbf{u}_i, \mathbf{u}_j)$ are calculated from a covariance model, which is usually built using the Linear Model of Regionalization (Journel and Huijbrets 1978; Goovaerts

1997). The weights that minimize the error variance are obtained by taking the partial first derivatives of Eq. 2.4 in relation to the weights and setting them to zero (Eq. 2.5):

$$\frac{\partial \sigma_E^2(\mathbf{u})}{\partial \lambda_i} = \sum_{i=1}^{n} \lambda_i \cdot C(\mathbf{u}_i, \mathbf{u}_j) - C(\mathbf{u}_i, \mathbf{u}) = 0$$
$$j = 1, \ldots, n, \tag{2.5}$$

which results in the simple kriging system (Eq. 2.6):

$$\sum_{i=1}^{n} \lambda_i \cdot C(\mathbf{u}_i, \mathbf{u}_j) = C(\mathbf{u}_i, \mathbf{u}) \quad j = 1, \ldots, n, \tag{2.6}$$

The substitution of Eq. 2.6 into the definition of the error variance (Eq. 2.4) results in the simple kriging variance (Eq. 2.7):

$$\sigma_E^2(\mathbf{u}) = C(0) - \sum_{i=1}^{n} \lambda_i \cdot C(\mathbf{u}_i, \mathbf{u}), \tag{2.7}$$

The simple kriging variance depends on the covariance model and the distance between the samples and the point $\mathbf{u}$ to be estimated. In general, as the samples get closer to the point to be estimated, their covariances with the point to be estimate $\mathbf{u}$ ($C(\mathbf{u}_i, \mathbf{u})$) increase and their weights increase. The result is that the simple kriging variance decreases.

## 2.3 Ordinary Kriging

The simple kriging estimate relies on a strong stationarity assumption, as the mean is considered known and constant over the entire area of study. In practice, datasets in the Earth Sciences do not have a constant mean. A location map of the samples often reveals areas of higher and lower values.

Ordinary kriging considers local variations of the mean, as it assumes that the mean is constant only inside the local neighborhood centered at the location $\mathbf{u}$ to be estimated. The local mean is considered unknown. Ordinary kriging filters the influence of the mean by forcing the kriging weights assigned to the surrounding data to sum one. In this context, the ordinary kriging estimator is written as a linear combination of the samples (Eq. 2.8):

$$z^*(\mathbf{u}) = \sum_{i=1}^{n} \lambda_i \cdot z(\mathbf{u}_i)$$

$$\sum_{i=1}^{n} \lambda_i = 1, \tag{2.8}$$

The ordinary kriging weights, similar to the simple kriging weights, also minimize the variance of the estimation error. The main difference is that the Lagrange formulism is used to add the constraint that the sum of the weights must be one. The ordinary kriging system is defined as follows (Eq. 2.9):

$$\begin{aligned} &\sum_{i=1}^{n} \lambda_i \cdot C(\mathbf{u}_i, \mathbf{u}_j) + \mu = C(\mathbf{u}_i, \mathbf{u}) \quad j = 1, \ldots, n \\ &\sum_{i=1}^{n} \lambda_i = 1, \end{aligned} \tag{2.9}$$

where $\mu$ is the Lagrange parameter. The substitution of Eq. 2.9 in the definition of the error variance (Eq. 2.4) results in the ordinary kriging variance (Eq. 2.10):

$$\sigma_E^2(\mathbf{u}) = C(0) - \sum_{i=1}^{n} \lambda_i \cdot C(\mathbf{u}_i, \mathbf{u}) - \mu, \tag{2.10}$$

## 2.4 Matrix Notation of Kriging

The matrix notation of the kriging system helps to understand the influence of data of different support in kriging and is reviewed. Using matrix notation, both the simple and ordinary kriging systems may be described using three matrixes:

- The left-hand-side (LHS) matrix **C**, which contains the covariances between the data;
- The weights vector **w**, which contains the kriging weights;
- The right-hand-side (RHS) matrix, **D**, which contains the covariances between the data and the point to be estimated.

Equation 2.11 describes the kriging system using matrix notation:

$$\mathbf{C} \cdot \mathbf{w} = \mathbf{D}, \tag{2.11}$$

The kriging weights are obtained by the multiplication of the inverse of the LHS matrix **C** by the RHS matrix **D**.

## 2.5 Block Kriging

In many applications, it is interesting to estimate the average value of some attribute $Z$ over a volume. For instance, in the mining industry, the decision whether the material is ore or waste is based on the average value of a block (also called *selective mining unity*—SMU) that has a volume in the space. The block size is related to the selectivity of the mining equipment and data spacing.

The term block kriging refers to the estimation of average values over a line, surface, or volume (Journel and Huijbregts 1978; Isaaks and Srivastava 1989; Goovaerts 1997). As long as the average is linear, the estimation of the average value over a block (or volume) may obtained as the average of $N$ point estimates. These point estimates occur at the $N$ points that discretize the block $V$ (Fig. 2.1). Traditionally, block kriging considers that the samples are at a quasi-point support, since the support of data is far smaller than the support of the block to be estimated.

Equation 2.12 defines the block estimate $z_V^*(\mathbf{u})$:

$$z_V^*(\mathbf{u}) = \frac{1}{N}\sum_{i=1}^{N} z^*(\mathbf{u}_i^{'}), \tag{2.12}$$

where $z_V^*(\mathbf{u})$ is the estimate of attribute $z$ over the block $V$ centered at location $\mathbf{u}$, $z^*(\mathbf{u}_i^{'})$ is the kriging estimate of attribute $z$ at the discretizing point $\mathbf{u}_i^{'}$, and $N$ is number of points used to discretize the block $V$.

This approach is computationally expensive since it demands the resolution of $N$ systems of linear equations to obtain a single block estimate. A more efficient approach is provided by the block kriging system, which obtains directly the block estimate by solving just one system of linear equations. Equation 2.13 defines the

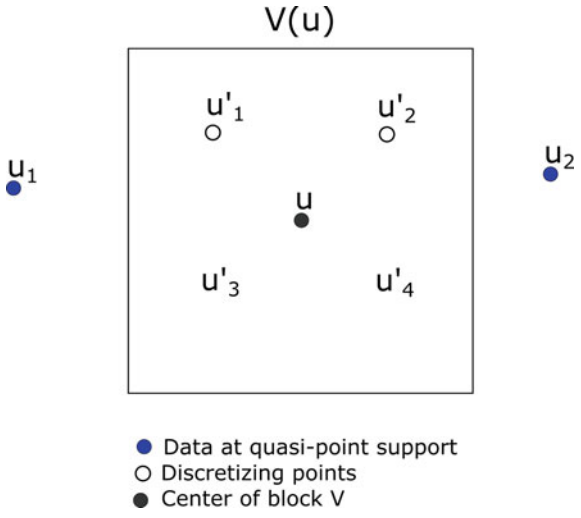


**Fig. 2.1** Scheme of block $V$ to be estimated with four discretizing points and two samples at quasi-point support

block kriging estimator:

$$z_V^*(\mathbf{u}) = \sum_{i=1}^{n} \lambda_i \cdot z(\mathbf{u}_i), \tag{2.13}$$

where $\lambda_i$ refers to the weight related to the datum at location $\mathbf{u}_i$ and $z(\mathbf{u}_i)$ refers to the datum at location $\mathbf{u}_i$, and $n$ is the number of data used for the estimation. The weights are obtained by the solving the block kriging system.

Similar to the traditional kriging system, the block kriging system contains three matrices: (i) the left-hand-side (LHS) matrix, which contains the covariances between the samples; (ii) the weight vector; and (iii) the right-hand side matrix, which contains the covariance between the samples and the block to be estimated. If the idea is to estimate a block (average value over a volume), the RHS matrix is modified to account for the volume to be estimated. In this case, the RHS matrix contains covariances point-to-block. Equation 2.14 defines the ordinary block kriging system:

$$\begin{aligned} &\sum_{i=1}^{n} \lambda_i \cdot C(\mathbf{u}_i, \mathbf{u}_j) \; + \; \mu = \overline{C}(\mathbf{u}_i, V) \quad j = 1, \ldots, n \\ &\sum_{i=1}^{n} \lambda_i = 1 \end{aligned} \tag{2.14}$$

The difference between the point and block kriging system is the construction of the RHS matrix. The RHS matrix of the "point" kriging system contains covariances point-to-point ($C(\mathbf{u}_i, \mathbf{u})$), while the RHS matrix of the block kriging system contains covariances point-to-block $\overline{C}(\mathbf{u}_i, V)$. The covariances point-to-block are obtained as a linear average of point-to-point covariances (Eq. 2.15):

$$\overline{C}(\mathbf{u}_i, V) = \frac{1}{N} \sum_{j=1}^{N} C(\mathbf{u}_i, \mathbf{u}_j^{'}), \tag{2.15}$$

where $N$ is the number of points that discretize the block $V$, $C(\mathbf{u}_i, \mathbf{u}_j^{'})$ is the covariance point-to-point between the sample located at $\mathbf{u}_i$ and the discretizing point $\mathbf{u}_j^{'}$. Figure 2.2 illustrates the calculation of the point-to-block covariance.

If the same samples are used to estimate all the $N$ discretizing points, the estimate obtained by block kriging is the same as the average of point kriging estimates of the $N$ discretizing points (Journel and Huijbregts 1978). The major benefit is that the block estimate is obtained directly by solving only one linear system of equations.

Equation 2.16 describes the ordinary block kriging variance:

$$\sigma_V^2(\mathbf{u}) = \overline{C}(V, V) - \sum_{i=1}^{n} \lambda_i \cdot \overline{C}(\mathbf{u}_i, V) - \mu, \tag{2.16}$$

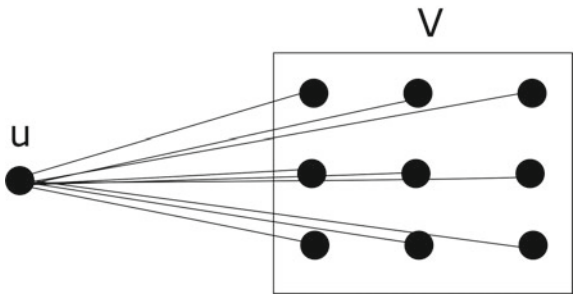


**Fig. 2.2** Scheme for calculating point-to-block covariance between point $u$ and block $V$. Each line represents a covariance point-to-point

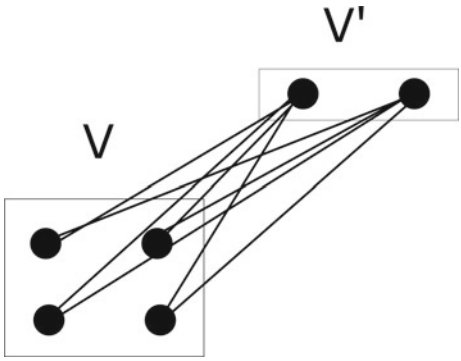


**Fig. 2.3** Scheme of calculation of block-to-block covariance between block $V$ and block $V'$. Each line represents a point-to-point covariance

where the block-to-block covariance[1] $\overline{C}(V, V)$, also called block variance, is approximated by the arithmetic average of point-to-point covariances defined between any point that discretize the block $V$ (Eq. 2.17):

$$\overline{C}(V, V) = \frac{1}{N^2} \sum_{i=1}^{N} \sum_{j=1}^{N} C(\mathbf{u}_i^{'}, \mathbf{u}_j^{'}), \tag{2.17}$$

Figure 2.3 shows a scheme of the calculation of the block-to-block covariances.

[1] One complicating factor when calculating the block variance is the zero effect (see Journel and Huijbregts 1978, p. 96). By definition, the value of the covariance for the distance of zero equals the variogram sill. However, this procedure tends to overestimate the block variance. The solution for this consists of slightly shifting one discretizing point when calculating the covariance between two discretizing points that are exactly at the same location.

## 2.6 Kriging with Data of Different Support

Considering that the data are defined at different support, the kriging system may be adapted to consider these differences. The data consist of a set of values defined over the supports $v_i$ $\{z(v_i); i = 1, \ldots, n\}$. Data defined over a volume are often called "block data." The block to be estimated is represented by $V$. Figure 2.4 illustrates the estimation of a block $V$ using data with different volumes. The grades of the data represent the average of the points that discretize the volumes.

One interesting property is that the volumes of either the data or the block to be estimated may have any shape. These volumes are represented by sets of discretizing points. For example, in Fig. 2.4, the support $v_1$ is a line that represents the average grade along a line (the line mimics samples from diamond drill holes), while $v_2$ represents the average grade of a mined area. The estimate of $z^*(V)$ is a linear combination of the samples defined over the volumes $v$ (Eq. 2.18):

$$z_V^*(\mathbf{u}) = \sum_{i=1}^{n} \lambda_i \cdot z(v_i), \tag{2.18}$$

When the support of the samples may not be considered as point or quasi-point support, the kriging system may be adapted to consider the support of the data. The adaptation consists of modifying the left-hand-side LHS, which contains the covariances between the data. When the data have different support, the LHS matrix is written using block-to-block covariances. The traditional block kriging system uses only point-to-point covariances in the LHS matrix (see Sect. 2.5). This property

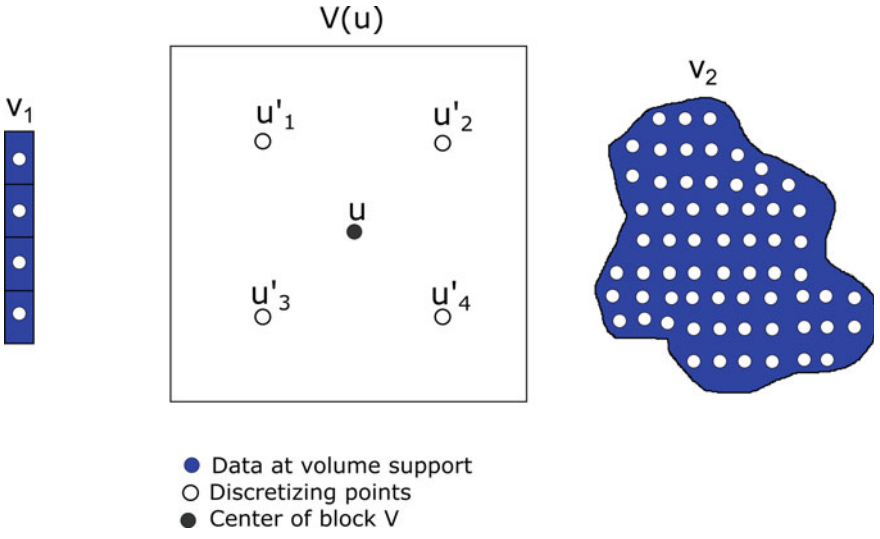


**Fig. 2.4** Scheme of block to be estimated $V$ using two samples of different support

is well described in the geostatistical literature (Journel and Huijbregts 1978; Isaaks and Srivastava 1989; Goovaerts 1997), but as far as the authors know has not been applied in the mineral industry. Equation 2.19 describes the ordinary kriging system with data of different support:

$$\begin{aligned}\sum_{i=1}^{n}\lambda_i\cdot\overline{C}(v_i,v_j)\ +\ \mu&=\overline{C}(v_i,V)\quad j=1,\ldots,n\\ \sum_{i=1}^{n}\lambda_i&=1,\end{aligned}\tag{2.19}$$

where $\overline{C}(v_i, v_j)$ is the block-to-block covariance between the block datum $v_i$ and the block datum $v_j$, and $\overline{C}(v_i, V)$ is the block-to-block covariance between the block datum $v_i$ and the block to be estimated $V$. The block-to-block covariance $\overline{C}(v_i, v_j)$ is the average of point-to-point covariances between all the points that discretize the block $v_i$ with all the points that discretize the block $v_j$ (Eq. 2.20):

$$\overline{C}(v_i,v_j)=\frac{1}{N_i}\cdot\frac{1}{N_j}\sum_{\alpha=1}^{N_i}\sum_{\beta=1}^{N_j}C(\mathbf{u}_\alpha^{'},\mathbf{u}_\beta^{'}),\tag{2.20}$$

where $N_i$ is the number of points $\mathbf{u}_\alpha^{'}$ that discretize the block $v_i$ and $N_j$ is the number of point $\mathbf{u}_\beta^{'}$ that discretize the block $v_j$. $C(\mathbf{u}_\alpha^{'},\mathbf{u}_\beta^{'})$ is the point-to-point covariance between the discretizing points $\mathbf{u}_\alpha^{'}$ and $\mathbf{u}_\beta^{'}$. Equation 2.21 describes the ordinary kriging variance using samples of different support:

$$\sigma_V^2(\mathbf{u})=\overline{C}(V,V)-\sum_{i=1}^{n}\lambda_i\cdot\overline{C}(v_i,V)-\mu,\tag{2.21}$$

## 2.7 Illustrative Example

This example shows the effect of considering the support of the data in kriging estimates (Bassani et al. 2018). The goal is to estimate the attribute at point $\mathbf{u}$ using two samples. One sample is considered to have a quasi-point support, and the other is defined over a volume $v$ in the space (Fig. 2.5). The volume of the block datum is centered at location $\mathbf{u}_1$, and the quasi-point datum is located at $\mathbf{u}_2$. The volume has equal size along the $X$ and $Z$ directions, and 16 discretizing points were used to calculate the average covariances. We compare kriging using only point-to-point covariances, which ignores the different support of the data, against kriging using average covariances. The estimations were performed using ordinary kriging.

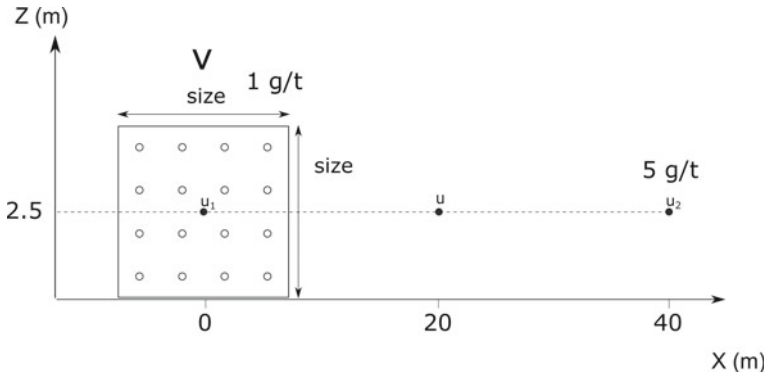


**Fig. 2.5** Estimation at point **u** using a datum at block-support centered at location $\mathbf{u}_1$ and a datum at a quasi-point support at $\mathbf{u}_2$

### *2.7.1 Sensitivity Analysis*

The estimate of the grade centered at **u** was carried out with different variogram models. The variogram model is defined at quasi-support. The effects on the weight of the block sample, on the estimate, and on the kriging variance, were measured. Since ordinary kriging was used, the weight of the quasi-point support sample is one minus the weight of the block sample.

Table 2.1 summarizes the sensitivity analysis. When one parameter was tested, the others remained unchanged for each comparative round. Four comparative rounds were performed to test four parameters (nugget effect, variogram range, variogram type, and block size). For example, the first comparative round tests the nugget effect ($C_0$). In this round, the variogram model consisted of the nugget effect tested plus a spherical structure with a fixed range of 60 m and contribution ($C_1$) of one minus the nugget effect tested.

**Table 2.1** Summary of parameters tested in the sensitivity analysis

| Comparative round | Parameter tested (variable) | Variogram model |
|---|---|---|
| 1st | Nugget effect ($C_0$) | $\gamma(h) = C_0 + C_1 \cdot \mathrm{Sph}\left(\frac{h}{60\,\mathrm{m}}\right)$ <br> $C_1 = 1 - C_0$ |
| 2nd | Range ($a$) | $\gamma(h) = 0.1 + 0.9 \cdot \mathrm{Sph}\left(\frac{h}{a}\right)$ |
| 3rd | Variogram type (vtype): Gaussian, spherical, exponential | $\gamma(h) = 0.1 + 0.9 \cdot \mathrm{vtype}\left(\frac{h}{60\,\mathrm{m}}\right)$ |
| 4th | Block size ($m$) | $\gamma(h) = 0.1 + 0.9 \cdot \mathrm{Sph}\left(\frac{h}{60\,\mathrm{m}}\right)$ |

### 2.7.2 *Effect of Nugget Effect*

Figures 2.6a–c show the influence of the nugget effect on the weight of the block sample, the estimate, and the kriging variance, respectively. As the nugget effect decreases, the weight of the block sample decreases for kriging with samples of different support (Fig. 2.6a). A low nugget effect means that the attribute is spatially continuous, and the volume represented by the block sample is redundant in terms of information. The result is that the kriging system considers this redundancy and decreases the weight of the block sample (this effect is known as the declustering property of kriging). In the case of low nugget effect, kriging ignoring the difference in supports, i.e., considering all data as quasi-point samples and kriging with samples of different support tend to generate similar estimates (Fig. 2.6b).

As the nugget effect increases, kriging loses its declustering property (Journel and Huijbregts 1978). The block sample becomes less redundant, and its weight increases (Fig. 2.6a). Moreover, the difference between the estimates (performed by kriging considering all samples as quasi-point and kriging with samples of different support) increases as the nugget effect increases (Fig. 2.6b). Mathematically, this difference occurs because the nugget effect highly influences the covariances block-to-block

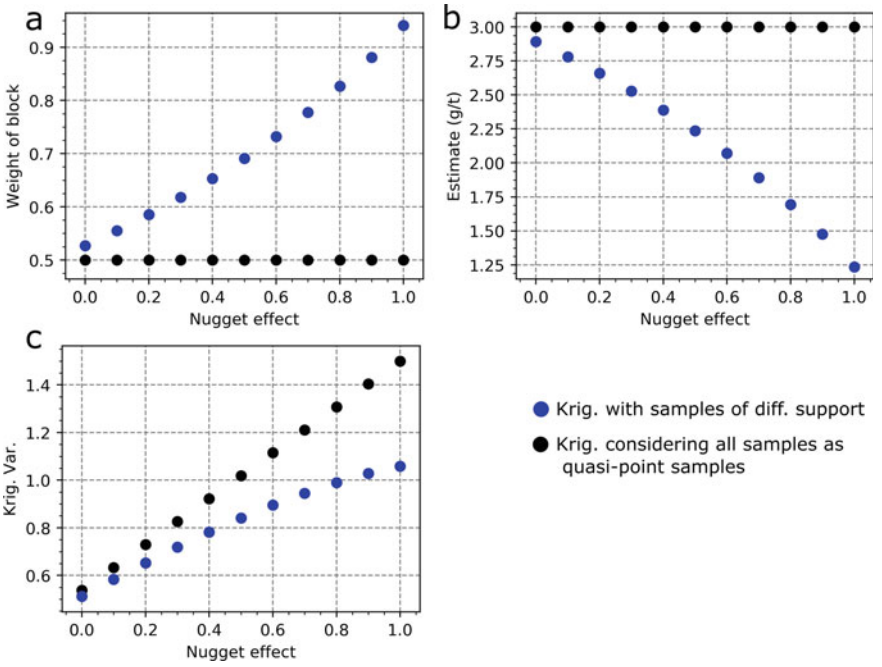


**Fig. 2.6** Effect of the nugget effect on **a** the weight of the block sample, **b** on the estimate, and **c** on the kriging variance. The variogram model used has two structures: a nugget effect and a spherical model with range equal to 60 m

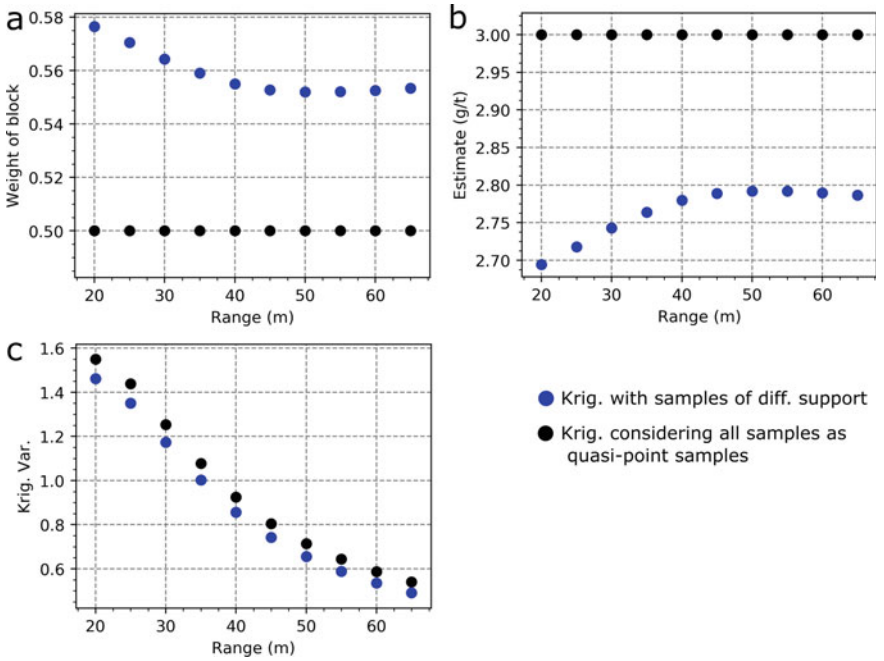


**Fig. 2.7** Effect of the variogram range **a** on the weight of the block sample, **b** on the estimate, and **c** on the kriging variance. The variogram model used has a nugget effect of 0.10 and a spherical model with a contribution of 0.90. The distance from the samples to the point to be estimated is 20 m

and point-block. When the nugget effect increases, the covariances block-to-block and point-to-block used in the LHS matrix decreases. The result is that the inverse of the LHS matrix produces higher weights for the block sample.

Overall, the kriging variances are lower for kriging with samples of different support (Fig. 2.6c). The average volume over the block sample represents more information than the grade at the center of the block, which is the case of kriging with quasi-point samples. In this context, the kriging variance is lower when the volume of the block is considered in the kriging system. As the nugget effect decreases, the block sample is redundant, and the kriging variance is similar for both estimation methods (kriging considering all samples as quasi-point and kriging with samples of different support).

### 2.7.3 Effect of Variogram Range

Overall, the weight of the block sample does not change much as the variogram range increases (Fig. 2.7a). The variogram range did not affect much the covariances point-to-block and block-to-block used in the kriging with samples of different support. The covariances block-to-block and point-to-block are mainly affected when the range is small compared to the block size. In this case, the ranges are longer than the block size (the block size is 5 m while the shortest range considered is 20 m).

As the variogram range increases, the weight of the block sample decreases (Fig. 2.7a). A long range means that the attribute is more spatially continuous and, thus, the block sample becomes redundant, and its weight decreases. As a result, the estimates of the two methods (kriging with quasi-point samples and kriging with samples of different support) become more similar (Fig. 2.7b).

The kriging variance decreased as the variogram range increased (Fig. 2.7c). As the variogram range increases, the phenomenon is more spatially continuous, and the kriging variance is expected to be lower.

### 2.7.4 Effect of Variogram Shape

Figure 2.8 shows the effect of the variogram type on the weight of the block sample, on the estimate, and on the error variance. Overall, the variogram type did not influence much the weight of the block sample, on the estimate, and on the kriging variance. The Gaussian variogram is more spatially continuous than the spherical variogram, which is more spatially continuous than the exponential variogram. As the phenomenon becomes more spatially continuous, the weight of the block sample decreases (Fig. 2.8a), and the kriging variance decreases. In this context, the Gaussian variogram model resulted in the lowest weight for the block sample (Fig. 2.8a) and kriging variance (Fig. 2.8c).

### 2.7.5 Effect of Support of the Samples

Figure 2.9 shows the effect of the block size on the weight of the block sample, on the estimate, and on the kriging variance. In general, the weight of the block sample increases as its size increases (Fig. 2.9a). This result occurs because the block size directly affects the covariances block-to-block used by kriging with samples of different support. As the block size increases, the covariances block-to-block in the LHS matrix tend to decrease. As a result, the inverse of the LHS matrix generates higher weights for the block sample.

As the block size diminishes, the block datum acts similarly to a quasi-point support sample. As a result, its weight is similar to the weight obtained by kriging

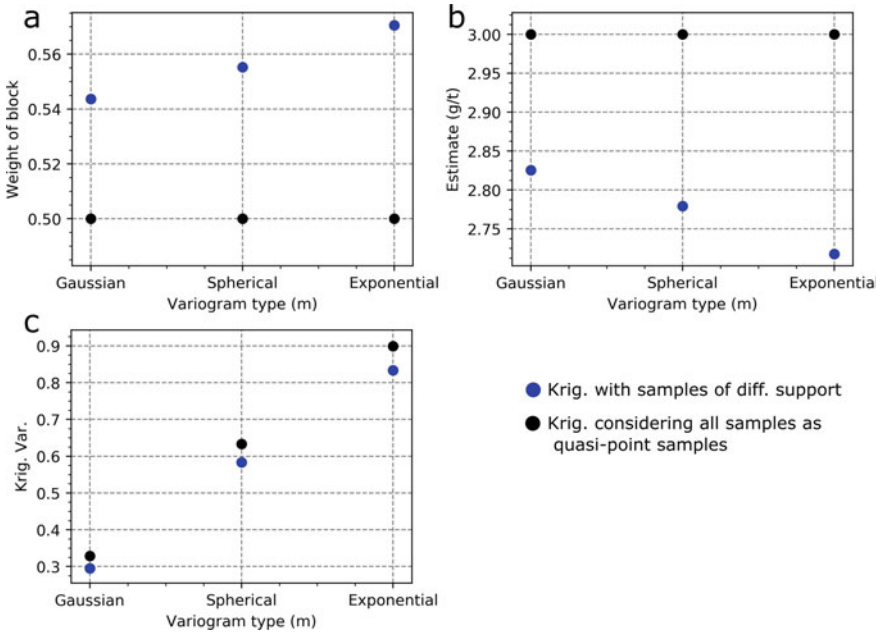


**Fig. 2.8** Effect of the variogram type **a** on the weight of the block sample, **b** on the estimate, and **c** on the kriging variance. The variogram model used has a nugget effect of 0.10 and a contribution of 0.90 in the second structure with range equal to 60 m

considering all samples as quasi-points. The result is that, with small block sizes, the estimates obtained by the two methods are similar (Fig. 2.9b).

Overall, the kriging variance decreases as the block size increases. As the block size increases, part of the block becomes closer to the point to be estimated. The result is that the kriging variance decreases (Fig. 2.9c).

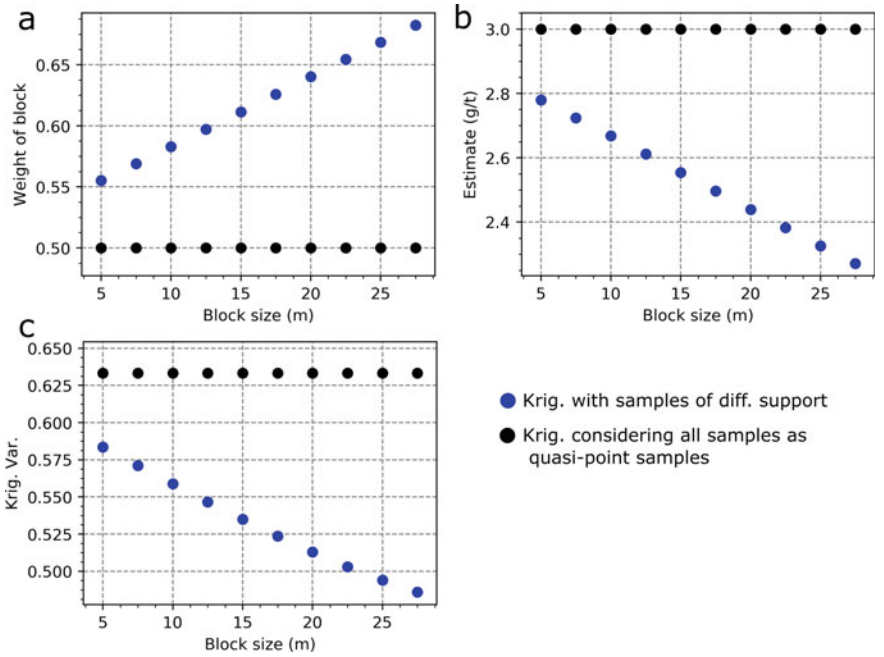


**Fig. 2.9** Effect of the block size **a** on the weight of the block sample, **b** on the estimate, and **c** on the kriging variance. The variogram model used has a nugget effect of 0.10 and a contribution of 0.90 in the second structure with range equal to 60 m

## References

Bassani MAA, Costa JFCL, Guaglianoni WC, Rubio RH (2018) Comparison between the indirect approach and kriging with samples of different support for estimation using samples of different length. Stoch Env Res Risk Assess 32(3):785–797

Deutsch CV, Journel AG (1998) GSLIB: geostatistical software library and user's guide. Oxford University Press, New York

Goovaerts P (1997) Geostatistics for natural resource evaluation. Oxford University Press, Oxford

Isaaks HE, Srivastava MR (1989) An introduction to applied geostatistics. Oxford University Press, Oxford

Journel AG, Huijbregts CJ (1978) Mining geostatistics. Academic Press, New York

# Chapter 3
# Simulation with Data of Different Support


## 3.1 Overview of Geostatistical Simulations

The estimates performed by kriging are built, so that each estimate considered individually (without considering the neighboring estimates) is "best." Best because the estimate minimizes the variance of the estimation error. However, when several estimated locations are considered together, such as an estimated grade model, the estimates do not represent the true spatial variability of the modeled variable. The map of the estimates has less variability than the modeled variable. The variance of the estimates is much lower than the variance of the data. This effect is called smoothing.

Conversely, geostatistical simulations generate a set of models with the same statistical and spatial characteristics of the data. The simulated models are known as realizations. The realizations, obtained by most algorithms, reproduce both the histogram and variogram of the data. The set of realizations also provides a measure of spatial uncertainty. For instance, areas where the simulated values differ a lot from one realization to another characterize areas of high uncertainty. The opposite is also true, i.e., low uncertainty areas are the areas where the simulated values are nearly the same at all realizations.

Estimated models should be used carefully when the variability of the data impacts the results where the models are applied. For instance, the ore tonnage of a deposit is often calculated based on the proportion of the blocks from the grade model above a given cut-off. The variance of the block model profoundly influences this proportion. A smooth grade model obtained by kriging leads to a biased tonnage estimation for ore. As a result, the ore tonnage derived from an estimated model differs from the actual ore tonnage. Geostatistical simulation overcomes this limitation of kriging. As the simulated models reproduce the variability of the phenomenon, the ore tonnage predicted by simulated models tends to be closer to the true tonnage (which is only known after complete extraction of the deposit) than the tonnage obtained by a kriged model.



M. A. Arcari Bassani and J. F. Coimbra Leite Costa, *Geostatistics with Data of Different Support Applied to Mining Engineering*, Topics in Mining, Metallurgy and Materials Engineering, https://doi.org/10.1007/978-3-030-80193-9_3

## 3.2 Data of Different Support in Geostatistical Simulation

### *3.2.1 Continuous Variables*

Many geostatistical simulation methods are found in the literature (Goovaerts 1997; Deutsch and Journel 1998; Chilés and Delfiner 1999). For continuous variables, the most common methods are the Sequential Gaussian Simulation (SGS), Sequential Indicator Simulation (SIS), and Turning Bands Simulation (TBS). The problem is that these simulation algorithms use a nonlinear transformation of the data, which is not adequate to integrate data of different support. A nonlinear transformation distorts the linear relationship between data of different support. In this context, the Direct Sequential Simulation (DSS) (Journel 1994; Oz et al. 2003; Soares 2001) is the appropriate method to integrate data of different support. DSS uses the data in their original units to condition the simulations and, thus, keeps the linear relationship between the data of different support.

### *3.2.2 Categorical Variables*

In the case of the simulation of categorical variables such as rock type, the suitable method to integrate data of different support is the Sequential Indicator Simulation (SIS) (Deutsch 2006) with the use of average covariances in the kriging system. Although SIS is not convenient for data of different support in case of continuous variables, the method works well for categorical ones. This suitability occurs because the average of indicators of categorical variables represents the mean probability of a given rock type over a volume in space. Many Gaussian methods are available for categorical variables, such as the Truncated Gaussian and Pluri-Gaussian Simulation (Xu and Journel 1993; Emery 2007; Armstrong et al. 2011). However, the Gaussian transformation used by these methods does not keep the linear relationship between the data of different support.

## 3.3 Direct Sequential Simulation with Data of Different Support

The Direct Sequential Simulation (DSS) algorithm is based on the theorem shown by Journel (1994). Journel (1994) demonstrated that, if the local cumulative distribution function (cdf) used at the sequential simulation has a mean and variance that equal the simple kriging estimate and variance, then the variogram is reproduced. The reproduction of the variogram does not depend on the shape of the local cdf.

The Direct Sequential Simulation algorithm consists of the following steps:

(i) Choose randomly a location **u** in the simulation grid and search for the nearby data and previously simulated nodes;
(ii) Calculate the mean and variance of the local conditional cumulative distribution function (ccdf) by simple kriging using the data and previously simulated nodes. The mean corresponds to the simple kriging estimate while the variance corresponds to the simple kriging variance;
(iii) Define a local ccdf whose mean and variance are equal to the simple kriging estimate and variance, respectively;
(iv) Draw a value from the local ccdf and add it to the dataset;
(v) Repeat steps i–iv until all the grid nodes are simulated.

The integration of data of different support in DSS involves kriging with samples of different support (using average covariances, as explained in Chap. 2) to obtain the mean and variance of the local ccdfs. There are many methods to sample from the local ccdf (Nowak and Srivastava 1997; Soares 2001; Oz et al. 2003). Among these methods, the Soares approach (Soares 2001) and the ccdf lookup table (Oz et al. 2003) tend to generate better results in terms of histogram reproduction. These two methods use the global reference histogram to sample the local ccdfs.

### *3.3.1 Sampling from the Local CCDF*

The main methods to sample from the local ccdf are the (i) Soares approach (Soares 2001) and (ii) ccdf lookup table (Oz et al. 2003). These two methods use the normal score transform to sample from the global histogram. In this context, the normal score transform is reviewed before the sampling methods are explained.

**Normal score transformation**

The normal score transformation $\varphi$ transforms the original data $z$ into Gaussian values $y$. The Gaussian values $y$ have a standard Gaussian distribution and are called normal scores. The normal score transformation (Deutsch and Journel 1998) is obtained by matching the quantiles of the cumulative distribution function (cdf) of the original data $F(z)$ with the quantiles of the standard Gaussian cdf $G(y)$.

Graphically, $F(z)$ may be interpreted as a function whose input is a value of the original data $z$ and the result is the corresponding cdf, which is between 0 and 1 (Fig. 3.1). Similarly, the function $G(y)$ calculates the cdf associated to a normal score $y$.

Equation 3.1 defines the normal score transformation $\varphi$:

$$y = \varphi(z) = G^{-1}[F(z)], \tag{3.1}$$

where $G^{-1}$ is the quantile function of the standard Gaussian distribution. The function $G^{-1}$ has as input a cdf value between 0 and 1 and returns the corresponding normal score value (Fig. 3.2):

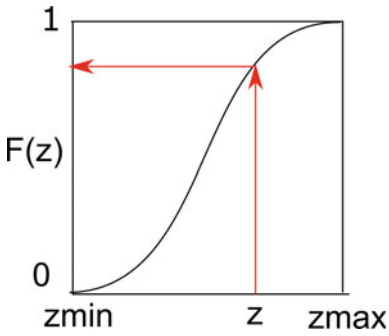


**Fig. 3.1** Scheme of the cumulative distribution function of the original data

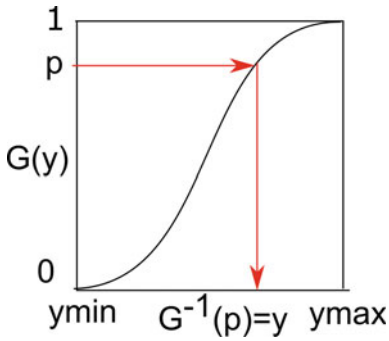


**Fig. 3.2** Scheme of the quantile function of the standard Gaussian cdf

The normal score transformation may be seen as a quantile–quantile table. Each quantile in the space of the original data matches a quantile in the Gaussian space (Fig. 3.3).

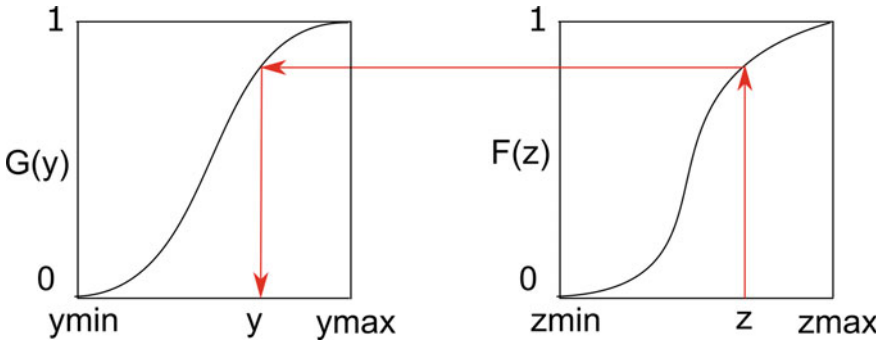


**Fig. 3.3** Scheme of the normal score transformation

**Soares approach**

The Soares approach (Soares 2001) to sample from the local ccdf is shown in Fig. 3.4 and involves the following steps:

(i) Calculate at the location **u** the mean $z^*(\mathbf{u})$ and variance $\sigma^2(\mathbf{u})$ of the local ccdf by simple kriging using the original and previously simulated data in the

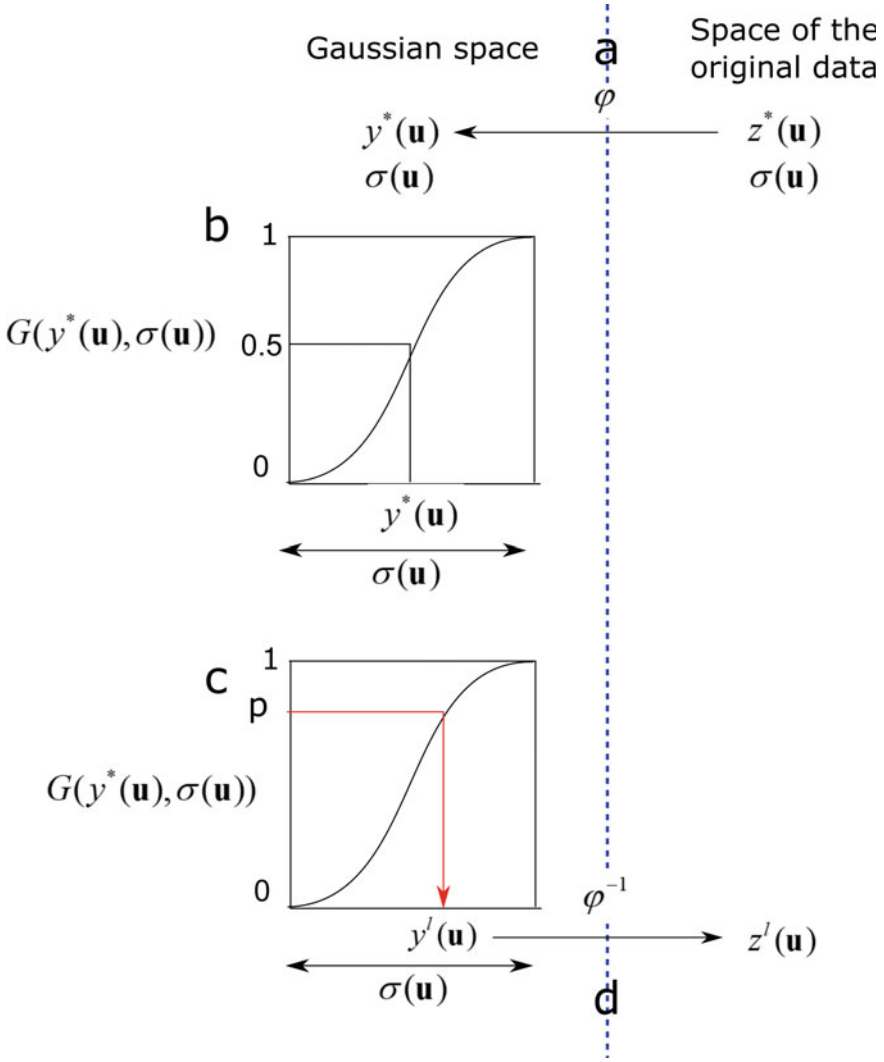


**Fig. 3.4** Scheme of a simulated value $z$ using the Soares approach: **a** normal score transform, **b** Gaussian cdf with mean and variance equals to $y^*(\mathbf{u})$ and $\sigma^2(\mathbf{u})$, **c** sampling from the local cdf, and **d** normal score transform back-transform

original units. $z^*(\mathbf{u})$ and $\sigma^2(\mathbf{u})$ are the simple kriging estimate and variance, respectively. $\sigma^2(\mathbf{u})$ is calculated using the standardized variogram of the original data, so that the sill is one;

(ii) Identify the Gaussian value $y^*(\mathbf{u})$ (Eq. 3.2) that matches the mean of the local ccdf $z^*(\mathbf{u})$ using the normal score transformation $\varphi$ (Fig. 3.4a):

$$y^*(\mathbf{u}) = \varphi(z^*(\mathbf{u})) \tag{3.2}$$

(iii) Build a Gaussian distribution at location $\mathbf{u}$ whose mean and variance are $y^*(\mathbf{u})$ and $\sigma^2(\mathbf{u})$, respectively (Fig. 3.4b);

(iv) Generate a random number $p$ between 0 and 1;

(v) Simulate a Gaussian value (Eq. 3.3) from the local Gaussian distribution using the random number $p$ (Fig. 3.4c):

$$y^l(\mathbf{u}) = G^{-1}(y^*(\mathbf{u}), \sigma(\mathbf{u}), p) \tag{3.3}$$

(vi) Transform the simulated Gaussian value $y^l(\mathbf{u})$ to the space of the original data using the normal score back-transformation $\varphi^{-1}$ (Eq. 3.4) (Fig. 3.4d):

$$z^l(\mathbf{u}) = \varphi^{-1}(y^l(\mathbf{u})) \tag{3.4}$$

(vii) Add the simulated value $z^l(\mathbf{u})$ to the dataset.

The steps i–vii are repeated until all the grid nodes are simulated.

The method proposed by Soares performs a nonlinear transformation of the estimate of the original data. This transformation may result in a degree of bias, which must be corrected. The following bias may occur (Eq. 3.5):

$$E[z^l(\mathbf{u})] \neq z^*(\mathbf{u}) \tag{3.5}$$

In other words, the average of the simulated values $E[z^l(\mathbf{u})]$ may differ from the estimate of the original data $z^*(\mathbf{u})$. In this context, Soares (2001) proposes a correction that involves the following steps:

(i) Estimate the average of the simulated value $E[z^l(\mathbf{u})]$ using Eq. 3.6:

$$E^*[z^l(\mathbf{u})] = \frac{1}{N}\sum_{i=1}^{N} z^l_{\mathrm{MC}}(\mathbf{u}) \tag{3.6}$$

where $z^l_{\mathrm{MC}}(\mathbf{u})$ is one the $N$ values obtained by Monte Carlo Simulation.

(ii) Correct the original simulated value using Eq. 3.7:

$$z^{l'}(\mathbf{u}) = z^l(\mathbf{u}) + \left[z^*(\mathbf{u}) - E^*[z^l(\mathbf{u})]\right] \tag{3.7}$$

Soares (2001) states that the impact of this correction is higher when the global histogram (used for the normal score transformation) has classes with low frequency.

**Ccdf lookup table**

Oz et al. (2003) propose to use a table of local ccdfs, which is called ccdf lookup table, to sample the simulated value. The process to obtain the ccdf lookup table involves the following steps:

(i) Build a list of all possible local Gaussian distributions. These Gaussian distributions are obtained by the combination of all possible means and standard deviations. In general, the values for the means are evenly spaced values between minus 3.5 and 3.5. For the standard deviation, the values are evenly spaced between zero and one. The combination of a mean $m$ with a standard deviation $\sigma$ results in a Gaussian distribution $G(m, \sigma)$;

(ii) For each Gaussian distribution generated at step i, a series of quantiles $p$ are used to simulate normal scores values $y^l$ (Eq. 3.8). Then, each simulated normal score value $y^l$ is transformed to the space of the original units $z^l$ using the normal score back-transform (Eq. 3.9):

$$y^l(p) = G^{-1}(m, \sigma, p) \tag{3.8}$$

$$z^l(p) = \varphi^{-1}(y^l(p)) \tag{3.9}$$

The result is a set of simulated values in the space of the original units. This set comprises a ccdf in the space of the original units. For each Gaussian distribution, there is a corresponding ccdf in the space of the original units.

(iii) Calculate the mean and variance of the ccdf in the space of the original units and store into a table;

The result is a ccdf lookup table in the space of the original units, with its mean and variance. During DSS, the local ccdf used is that whose mean and variance equal the simple kriging estimate and variance, respectively.

Figure 3.5 shows how a local ccdf in the space of the original units is built starting from a local Gaussian distribution using only four quantiles. In practice, one hundred or more quantiles are used.

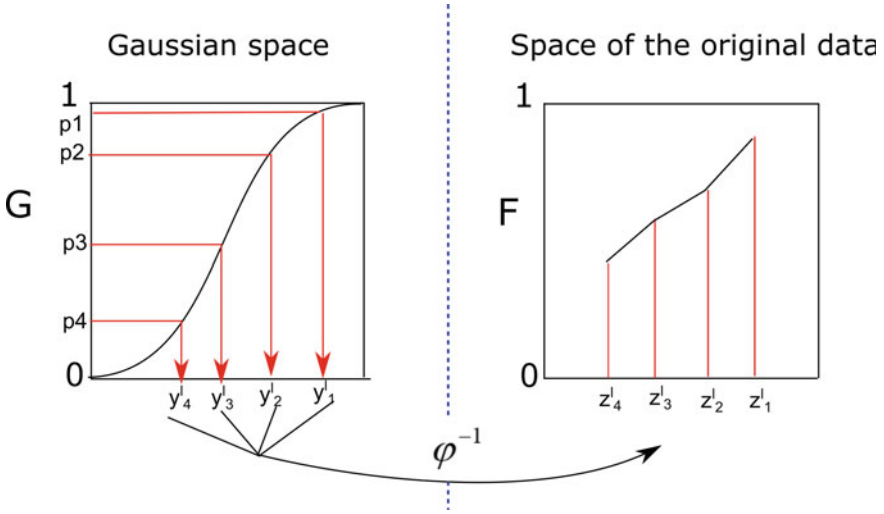


**Fig. 3.5** Scheme of obtaining a cdf in the space of the original units by transforming a series of quantiles in the Gaussian space

## 3.4 Sequential Indicator Simulation with Data of Different Support

### *3.4.1 Indicators for Categorical Variables*

Consider $K$ categories that are mutually exclusive (only one category may prevail at a given location). The indicator approach requires that the dataset is transformed into a series of $K$ indicators. Equation 3.10 defines how the indicators are obtained:

$$i(\mathbf{u}_i; k) = \begin{cases} 1 \text{ if category } k \text{ prevails at location } \mathbf{u}_i \\ 0 \text{ otherwise} \end{cases}, \tag{3.10}$$

where $i(\mathbf{u}_i; k)$ is the indicator for category $k$ at location $\mathbf{u}_i$. The indicator represents the probability that a given category prevails at a given location. In the case of *hard data*,[1] the indicator is 1 if the category prevails or zero if does not prevail. For instance, consider that a rock type is classified as either ore or waste. A sample that is ore results in an indicator of 1 for the ore category. In other words, there is 100% probability that the sample is ore.

[1] The term hard data refers to data that do not have sampling errors in the geostatistical literature.

### 3.4.2 Indicator Kriging

Indicator kriging for categorical variables estimates the probability that category $k$ prevails at location $\mathbf{u}$. Many kriging algorithms may be used (simple kriging, ordinary kriging, cokriging, simple kriging with local mean). These kriging algorithms are well detailed in the literature (Goovaerts 1997; Deutsch and Journel 1998; Chilés and Delfiner 1999). Here, we focus on the integration of data of different support for categorical variables.

The simple kriging estimator assumes that the mean probability $p_k$ is known and constant over all the area of interest. Equation 3.11 defines the simple indicator kriging estimator:

$$i(\mathbf{u};k)^* = p_k + \sum_{i=1}^{n} \lambda_i \cdot [i(\mathbf{u}_i;k) - p_k] \tag{3.11}$$

where $i(\mathbf{u}_\alpha;k)^*$ is the estimate (obtained by simple kriging) of the probability that category $k$ prevails at location $\mathbf{u}$, $\lambda_i$ is the simple kriging weight associated to the indicator $i(\mathbf{u}_i;k)$, and $p_k$ is the mean probability for category $k$. The weights are obtained by the resolution of the simple kriging system.

Equation 3.12 defines the ordinary kriging estimator:

$$i(\mathbf{u};k)^* = \sum_{i=1}^{n} \lambda_i \cdot i(\mathbf{u}_i;k) \tag{3.12}$$

where $i(\mathbf{u}_\alpha;k)^*$ is the estimate of the probability that category $k$ prevails at location $\mathbf{u}$, $\lambda_i$ is the ordinary kriging weight associated to the indicator. The weights are obtained by the resolution of the simple kriging system.

The integration of data of different support for indicator kriging involves using average covariances to build the indicator kriging system, as explained in Chap. 2. The LHS and RHS matrices are built using covariances point-to-block and block-to-block, so that the difference of support between the samples is considered.

### 3.4.3 Sequential Indicator Simulation with Data of Different Support

The sequential indicator with data of different support (Deutsch 2006) assumes that the data defined over a volume represents the average probability that a given category prevails over this volume. The data that represent average values over volumes or areas are called block data. For instance, consider that the proportion of ore over a volume of $5 \times 5 \times 2$ m$^3$ is 60%. In this case, the indicator data for this volume is 0.60.

The sequential indicator simulation with data of different support involves the following steps:

(i) Choose randomly a location **u** in the simulation grid and search for nearby data and previously simulated nodes;
(ii) Calculate the probability that each category $k$ prevails at location **u** by indicator kriging $[i(\mathbf{u}; k)^*]$. Simple or ordinary kriging may be used. The indicator kriging system is built using average covariances so that the difference of support between the samples is considered;
(iii) Define any order of the $K$ categories and build a cdf-type function by adding the probabilities estimated at step ii (Eq. 3.13):

$$F(\mathbf{u}; k')^* = \sum_{k=1}^{k'} i(\mathbf{u}; k)^* \tag{3.13}$$

(iv) Draw a value from the local ccdf and add it to the dataset.

The steps i–iv are repeated until all the grid nodes are simulated.

## References

Armstrong M, Galli A, Beucher H, Loc'h G, Renard D, Doligez B, Eschard R, Geffroy F (2011) Plurigaussian simulations in geosciences. Springer Science & Business Media, Berlin

Chilés JP, Delfiner P (1999) Geostatistics: modeling spatial uncertainty. Wiley, New York

Deutsch CV (2006) A sequential indicator simulation program for categorical variables with point and block data: blockSIS. Comput Geosci 32(10):1669–1681

Deutsch CV, Journel AG (1998) GSLIB: geostatistical software library and user's guide. Oxford University Press, New York

Emery X (2007) Simulation of geological domains using the plurigaussian model: new developments and computer programs. Comput Geosci 33(9):1189–1201

Goovaerts P (1997) Geostatistics for natural resource evaluation. Oxford University Press, Oxford

Journel AG (1994) Modeling uncertainty: some conceptual thoughts. Geostatistics for the next century. Springer, Dordrecht, pp 30–43

Nowak MS, Srivastava RM (1997) A geostatistical conditional simulation algorithm that exactly honours a predefined grade-tonnage curve. In: Geostatistics Wollongong vol 96, pp 669–682

Oz B, Deutsch CV, Tran TT, Xie Y (2003) DSSIM-HR: A FORTRAN 90 program for direct sequential simulation with histogram reproduction. Comput Geosci 29(1):39–51

Soares A (2001) Direct sequential simulation and cosimulation. Math Geol 33(8):911–926

Xu W, Journel AG (1993) GTSIM: gaussian truncated simulations of reservoir units in a W Texas carbonate field. SPE 27412:3–6

# Chapter 4
# Change of Support in the Variogram


The use of average covariances for geostatistical simulation requires the variogram model at point support. However, obtaining the variogram at point support is a challenge when the samples have completely different supports. The goal of this chapter is to show how to change the support of the variogram. Changing the support of the variogram means that we can obtain a variogram at block support starting from a variogram at point support and vice-versa.

The technical terms for the change of support in the variogram are variogram regularization and deconvolution. Variogram regularization means obtaining a variogram at block support from a variogram at point support (this process is also called variogram upscaling). Variogram deconvolution is the opposite: obtaining a variogram at point support from a variogram at block support (this process is also called variogram downscaling). The methods for variogram regularization and deconvolution are shown in this chapter.

## 4.1 Experimental Variogram for Data of Different Support

Equation 4.1 defines the experimental variogram for point-support samples:

$$\hat{\gamma}(\mathbf{h}) = \frac{1}{2N(\mathbf{h})} \sum_{i=1}^{N(\mathbf{h})} [z(\mathbf{u}_i) - z(\mathbf{u}_i + \mathbf{h})]^2, \tag{4.1}$$

where $N(\mathbf{h})$ is the number of pairs for samples separated by the vector $\mathbf{h}$, $z(\mathbf{u}_i)$ is the datum located at $\mathbf{u}_i$, and $z(\mathbf{u}_i + \mathbf{h})$ is the datum located at $\mathbf{u}_i + \mathbf{h}$. Similarly, Eq. 4.2 defines the experimental variogram for samples of different support (Goovaerts 2008):



M. A. Arcari Bassani and J. F. Coimbra Leite Costa, *Geostatistics with Data of Different Support Applied to Mining Engineering*, Topics in Mining, Metallurgy and Materials Engineering, https://doi.org/10.1007/978-3-030-80193-9_4

$$\hat{\gamma}(\mathbf{h}) = \frac{1}{2N(\mathbf{h})} \sum_{i=1}^{N(\mathbf{h})} \left[ z_{v_i}(\mathbf{u}_i) - z_{v_{i+\mathbf{h}}}(\mathbf{u}_i + \mathbf{h}) \right]^2 \tag{4.2}$$

The use of samples of different support to calculate the experimental variogram may be questioned (Journel 1986). In theory, samples with different support have different variances. These different variances lead to different sills for the variogram model. In this context, the practitioner should select a subset of similar support samples to calculate the experimental variogram. The problem occurs when there are few data of similar support. In this case, the experimental variogram becomes noisy and does not show spatial continuity. From a practical view, the samples of different support aid to infer the spatial continuity model and may be used for the experimental variogram. The idea is to use all available information to infer the spatial continuity model as best as possible.

## 4.2 Variogram Regularization for Blocks of Regular Shape

Under the stationarity hypothesis, the point-support variogram and the variogram at block support are related by Eq. 4.3 (Journel and Huijbregts 1978, p. 77):

$$\gamma_v(\mathbf{h}) = \bar{\gamma}(v, v_{\mathbf{h}}) - \bar{\gamma}(v, v), \tag{4.3}$$

where $\gamma_v(\mathbf{h})$ is the variogram at block support at a distance $\mathbf{h}$, $\overline{\gamma}(v, v_{\mathbf{h}})$ is the average variogram between the block $v$ and the block $v$ separated by a distance $\mathbf{h}(v_{\mathbf{h}})$. The term $\overline{\gamma}(v, v)$ is the average variogram within the block $v$ and is commonly called *gammabar*. Equation 4.4 shows the calculation of the *gammabar* $\overline{\gamma}(v, v)$:

$$\bar{\gamma}(v, v) = \frac{1}{N^2} \sum_{i=1}^{N} \sum_{j=1}^{N} \gamma(\mathbf{u}_i^{'}, \mathbf{u}_j^{'}), \tag{4.4}$$

where $N$ is the number of discretizing points of the block $v$. Equation 4.5 shows the calculation of the variogram between blocks $\overline{\gamma}(v, v_{\mathbf{h}})$:

$$\bar{\gamma}(v, v_{\mathbf{h}}) = \frac{1}{N_i N_j} \sum_{i=1}^{N_i} \sum_{j=1}^{N_j} \gamma(\mathbf{u}_i^{'}, \mathbf{u}_j^{'}), \tag{4.5}$$

where $N_i$ is the number of discretizing points of the block $v$ and $N_j$ is the number of discretizing points of the block $v_{\mathbf{h}}$. The presented relations assume that all the blocks have the same geometric shape. Goovaerts (2008) showed a general formula of variogram regularization, which is suitable for blocks of irregular shapes. This formula is shown in Sect. 4.3.

## 4.3 Variogram Regularization for Blocks of Irregular Shape

When all the blocks have the same shape, the term $\overline{\gamma}(v, v)$ is constant. However, when the blocks have different shapes, the term $\overline{\gamma}(v, v)$ depends on the distance $\mathbf{h}$ and on the shapes of the volumes considered. Equation 4.6 shows the variogram regularization for blocks with different shapes and sizes (Goovaerts 2008):

$$\gamma_v(\mathbf{h}) = \bar{\gamma}_{\mathbf{h}}(v, v_{\mathbf{h}}) - \bar{\gamma}_{\mathbf{h}}(v, v), \tag{4.6}$$

The term $\bar{\gamma}_{\mathbf{h}}(v, v)$ is the arithmetic average of *gammabars* for blocks separated by a distance $\mathbf{h}$ (Eq. 4.7):

$$\bar{\gamma}_{\mathbf{h}}(v, v) = \frac{1}{2N(\mathbf{h})} \sum_{i=1}^{N(\mathbf{h})} \left[\bar{\gamma}(v_i, v_i) + \bar{\gamma}(v_{i+\mathbf{h}}, v_{i+\mathbf{h}})\right], \tag{4.7}$$

where $N(\mathbf{h})$ is the number of pairs of blocks separated by a distance $\mathbf{h}$. $\bar{\gamma}(v_i, v_i)$ is the gammabar, calculated by Eq. 4.4.

Equation 4.8 defines the calculation of $\bar{\gamma}_{\mathbf{h}}(v, v_{\mathbf{h}})$:

$$\bar{\gamma}_{\mathbf{h}}(v, v_{\mathbf{h}}) = \frac{1}{N(\mathbf{h})} \sum_{i=1}^{N(\mathbf{h})} \bar{\gamma}(v_i, v_{i+\mathbf{h}}), \tag{4.8}$$

where $\overline{\gamma}_{\mathbf{h}}(v, v_{\mathbf{h}})$ is the arithmetic average of variograms between blocks separated by the distance $\mathbf{h}$. The term $\bar{\gamma}(v_i, v_{i+\mathbf{h}})$ is obtained by Eq. 4.5.

## 4.4 Variogram Deconvolution

Journel and Huijbregts (1978, p. 90) proposed a method to obtain the point-support variogram considering that the samples are measured at a volume $v$. This process is called variogram deconvolution. The method involves the following steps:

1. Define an initial point-support variogram model $\gamma(\mathbf{h})$ using the experimental variogram at block support $\hat{\gamma}_v(\mathbf{h})$;
2. Compute the theoretical variogram model at block support $\gamma_v(\mathbf{h})$ using Eq. 4.3 and compare it against the experimental points $\hat{\gamma}_v(\mathbf{h})$;
3. Adjust the point-support variogram model's parameters $\gamma(\mathbf{h})$ until the theoretical model $\gamma_v(\mathbf{h})$ fits the experimental points $\hat{\gamma}_v(\mathbf{h})$.

This method has been successfully applied by Goovaerts (2008) in a case study where the blocks had different sizes and shapes. Often, the central gap to integrate data of different support in kriging is inferring the point-support variogram model.

The method proposed by Journel and Huijbregts (1978) and reviewed here shows how to fill this gap.

## References

Goovaerts P (2008) Kriging and semivariogram deconvolution in the presence of irregular geographical units. Math Geosci 40(1):101–128
Journel AG (1986) Geostatistics: models and tools for the earth sciences. Math Geol 18(1):119–140
Journel AG, Huijbregts CJ (1978) Mining geostatistics. Academic Press, New York

# Chapter 5
# Case Study of Kriging with Data of Different Support


## 5.1 Dataset Presentation

The dataset contains 686 drill holes located on a relatively regular grid of 200 m × 200 m spacing along the East ($X$) and North ($Y$) directions. This dataset was used by Bassani and Costa (2016). The original $Z$ coordinates were converted into stratigraphic coordinates. The stratigraphic coordinate is the $Z$ coordinate of the sample's centroid minus the $Z$ coordinate of the top of the seam used as a reference. Several authors discuss the importance of stratigraphic coordinates for geostatistical modeling in tabular deposits (Deutsch 2002; Pyrcz and Deutsch 2014; Rubio et al. 2015).

The variable of interest is the fraction of the total sample mass retained at the 14 # sieve aperture (REC14). This variable represents the proportion of coarse fragments and is essential to predict the amount of concentrated ore after the washing process. REC14 is an additive variable, like grades, so the methods presented here are also adequate for grades.

REC14 was sampled roughly at the nominal length of 0.5 m. To demonstrate the technique, which regards samples of different lengths, half of the 686 drill holes were selected randomly. In these selected drill holes, REC14 was composited by the total intercepted seam. The composite length corresponds to the ore thickness, and the composite grade represents the average REC14 over this thickness. The final dataset contains 343 drill holes with one sample intercepting the total ore thickness (blue points in Fig. 5.1) plus 343 drill holes with samples whose length is nearly 0.5 m (red points in Fig. 5.1). The dataset imitates a dataset whose samples came from different campaigns with different sampling lengths.

Figure 5.2a shows the length-weighted histogram of REC14. The distribution is roughly symmetric around the mean, and the coefficient of variation is low (0.19). The coefficient of variation is much lower than one, indicating that the distribution does not contain extreme values that predominantly affect the mean. The drill holes are regularly spaced, so these statistics are representative of the study area. Figure 5.2b shows the QQ-plot between the original and declustered data. The data



M. A. Arcari Bassani and J. F. Coimbra Leite Costa, *Geostatistics with Data of Different Support Applied to Mining Engineering*, Topics in Mining, Metallurgy and Materials Engineering, https://doi.org/10.1007/978-3-030-80193-9_5

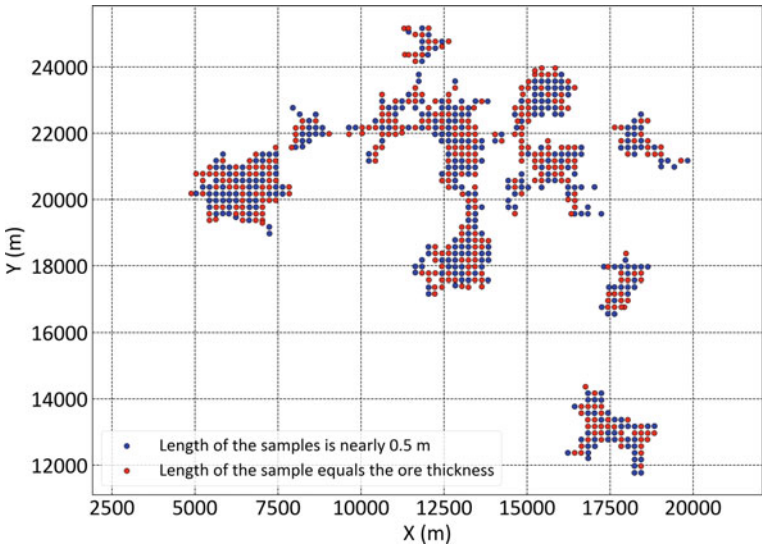


**Fig. 5.1** Location map of the samples

were declustered using the nearest neighbor estimate, which approximates the polygonal declustering method (Isaaks and Srivastava 1989). The points in Fig. 5.2b are close to the line $y = x$ and show that the two distributions are similar, as expected.

Figure 5.2c shows the histogram of the length of the samples. The length of the samples ranges between 0.25 and 7.88 m. Since about 80% of the samples are short, whose lengths are between 0.25 and 0.75 m, the geomodeler may feel motivated to retain only these short samples (all of them at equivalent support) for estimation. However, keeping only the short samples results in discarding 50% of the drill holes. This loss of information is likely to worsen the estimates.

## 5.2 Variogram Analysis and Modeling

The point-support variogram model was obtained by the variogram deconvolution method described in Chap. 4. Figure 5.3a, b shows the experimental variogram along with the horizontal and vertical directions. Both the quasi-point (samples with a length of 0.5 m) and block samples (samples longer than 0.5 m) were used for the experimental variogram, which is called block experimental variogram (blue dots in Fig. 5.3). The block variogram (dashed green line in Fig. 5.3) was obtained by the regularization of the point-support variogram model (black line in Fig. 5.3). The goal is to minimize the difference between the block experimental variogram and the block variogram.

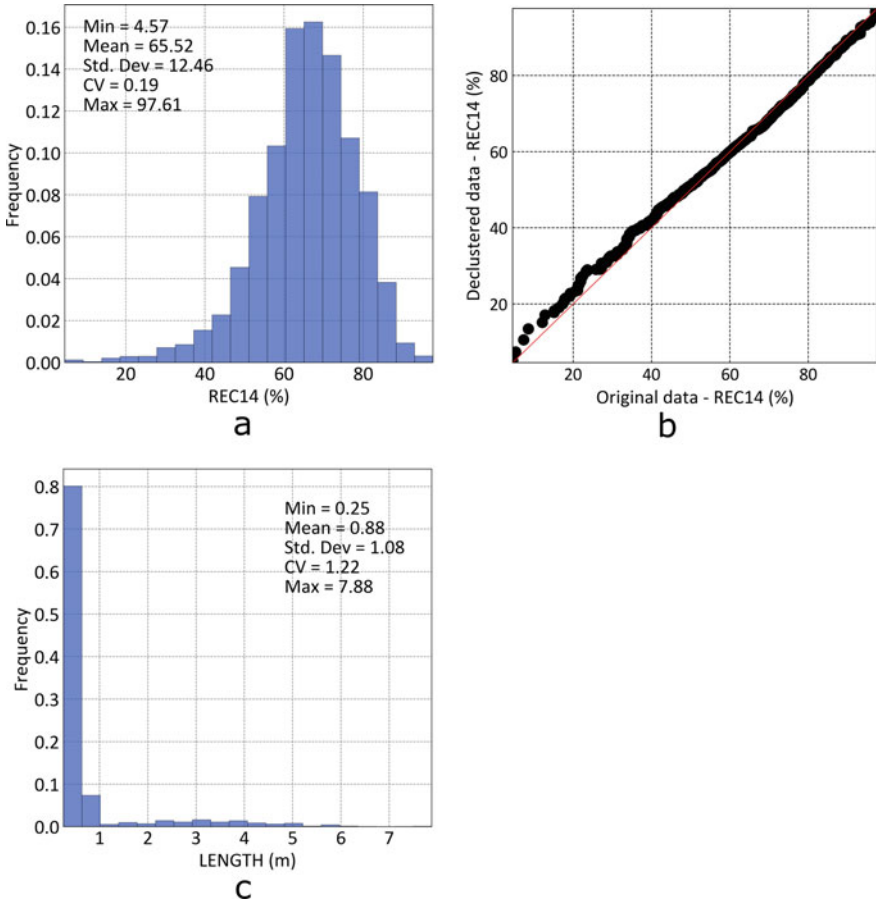


**Fig. 5.2** **a** Histogram of REC14, **b** QQ-plot between the original and declustered data, and **c** histogram of the length of the samples

Equation 5.1 describes the point-support variogram model of REC14. The variogram is standardized so that the sill equals one.

$$\gamma(\mathbf{h}) = 0.11 + 0.59 \cdot \mathrm{Sph}\left(\frac{\mathrm{NS}}{300\,\mathrm{m}}, \frac{\mathrm{EW}}{300\,\mathrm{m}}, \frac{\mathrm{vert.}}{3\,\mathrm{m}}\right) + 0.30 \cdot \mathrm{Sph}\left(\frac{\mathrm{NS}}{5000\,\mathrm{m}}, \frac{\mathrm{EW}}{5000\,\mathrm{m}}, \frac{\mathrm{vert.}}{7\,\mathrm{m}}\right) \tag{5.1}$$

The variable of interest is isotropic on the horizontal plane, and the direction of minor spatial continuity is vertical. This variogram model is consistent with the geology of the deposit. Figure 5.4 shows a location map of the samples colored

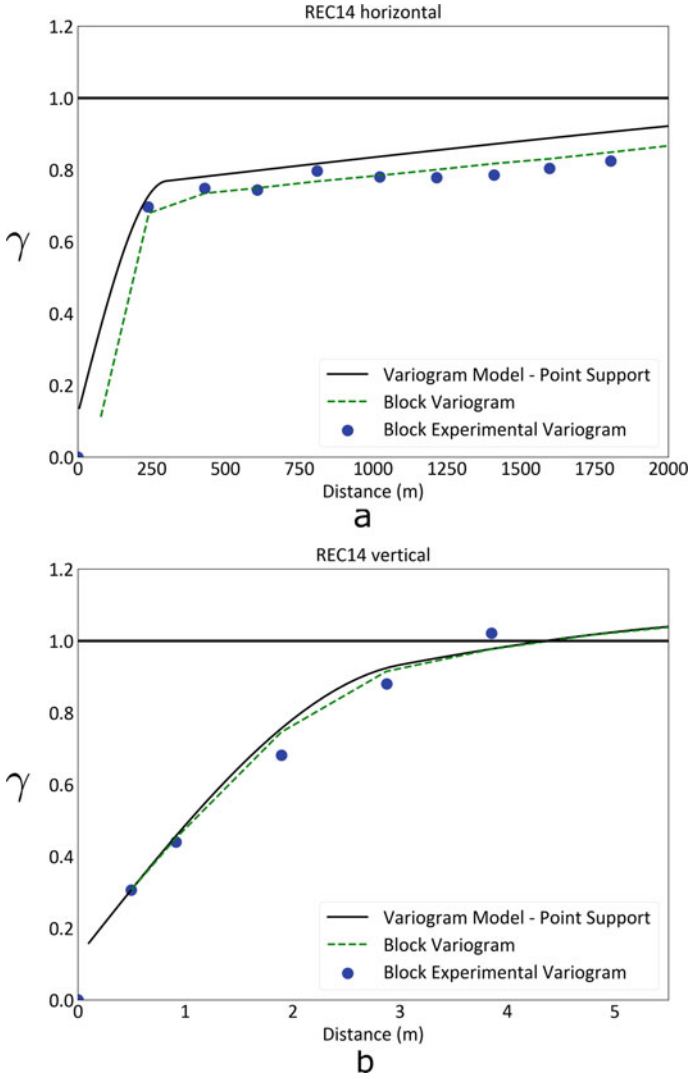


**Fig. 5.3** Experimental variogram, variogram model at point support, and block variogram along with the **a** horizontal and **b** vertical directions

by the variable of interest. The samples do not show an evident anisotropy and are consistent with the variogram model.

The variable of interest has a short range along the vertical direction. If the attribute is spatially discontinuous (i.e., presents high nugget effect and short range), kriging with samples of different support results in higher weights to the long samples compared to kriging using point covariances. This effect is observed in the simple example shown in Chap. 2. As the ratio length of the sample/range of the variogram

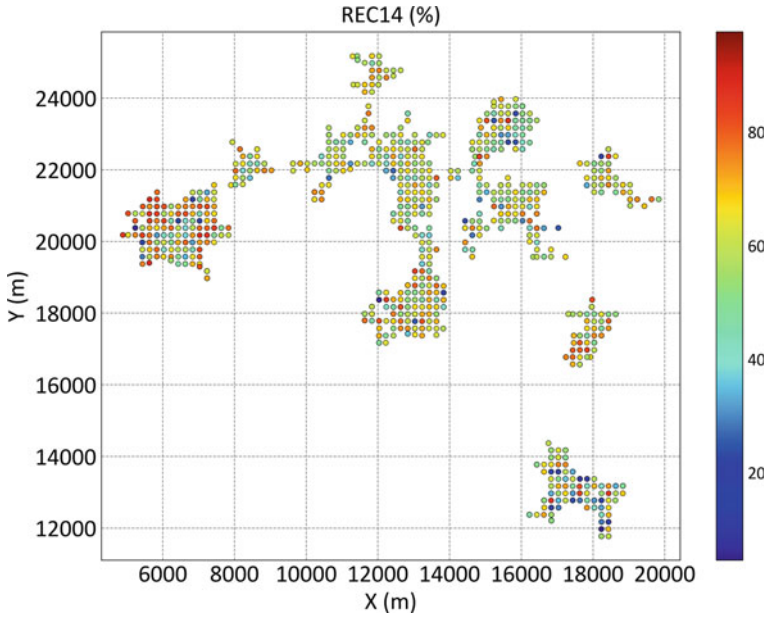


**Fig. 5.4** Location map of the samples colored by REC14

increases, the covariance block-to-block tends to decrease, and the kriging weights increase.

## 5.3 Estimation and Validation

Ordinary kriging with samples of different support was used to estimate REC14. The drill hole samples were discretized along the direction of the drill hole (vertical direction). The discretization spacing corresponds to 0.5 m, which is the length of the shortest samples. This length represents quasi-point support. These discretization points were used to calculate the covariances point-to-block and block-to-block between the samples.

The block model consists of blocks whose dimensions are 50 m × 50 m × 0.5 m along the $X$, $Y$, and $Z$ directions. The block discretization was set to 5 × 5 × 1. The estimates were limited for the blocks inside the geological model.

The model was checked by visual inspection and swath plots. The visual inspection consists of plotting and analyzing the grade model and the data using the same color scale. The data should justify the grade model.

The swath plot starts by dividing the area of interest into a series of swaths. Within each swath, the average of the estimates is compared against the average of

the declustered data. In this case, the data were declustered using the nearest neighbor estimate.

## 5.4 Comparison Against Kriging Using Point Covariances

Kriging with different support samples was compared against kriging using point covariances, which disregards the difference of support between the samples. In this case, all the samples are considered to have quasi-point support. The left-hand-side matrix of the kriging system is filled only with point covariances. The comparison was performed with cross-validation.

Cross-validation allows the practitioner to compare the actual and estimated values to minimize their differences. Cross-validation starts by removing one sample at a particular location. Then, the estimate is performed at that location using the remaining samples. The procedure is repeated for all the locations of the dataset. The same parameters used to estimate the block model are used for the cross-validation. Last, the estimation error (the difference between the estimated and true values), the mean absolute error, and the mean squared error were calculated. The mean estimation error measures the accuracy of the estimates. The mean absolute error, the mean squared error, and the standard deviation of the error are used to measure the precision of the estimates.

## 5.5 Results

### *5.5.1 Estimates*

Figure 5.5 shows a plan view of the estimates. The West part of the block model shows high grades, matching the high-grade samples in this region (see Fig. 5.4).

Figure 5.6 shows a plan view of the block model and the samples with the same color scale. The high-grade blocks are close to the high-grade samples, as expected.

The swath plots show that the block model reproduced the trend of the data along the $X$, $Y$, and $Z$ directions (see Figs. 5.7a–c). Along with the three directions, the local mean of the estimates is similar to the local mean of the declustered data. The swath plot also shows that the estimates are not always above or always below the declustered data.

The swath plot along the $Z$ direction (Fig. 5.7c) showed discrepancies between the declustered mean and the mean of the estimates for the lowest elevations. This discrepancy occurred because the stratigraphic coordinates are based on the $Z$ coordinate of the seam's top. Figure 5.8 shows a cross section of the drill holes with the stratigraphic coordinates. The areas of lower elevations have fewer samples than the

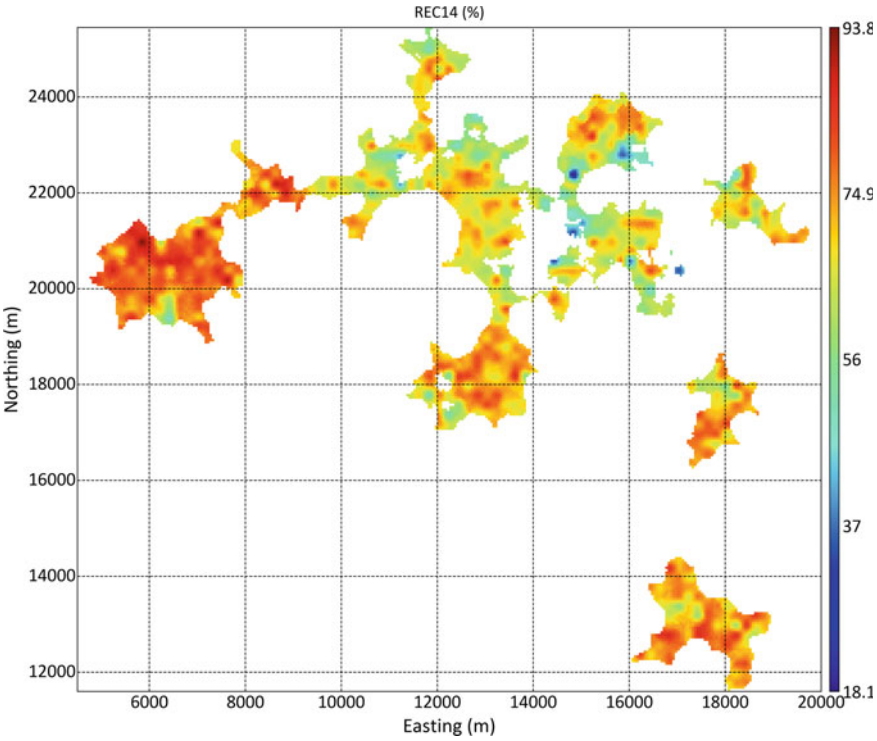


**Fig. 5.5** Block model estimates

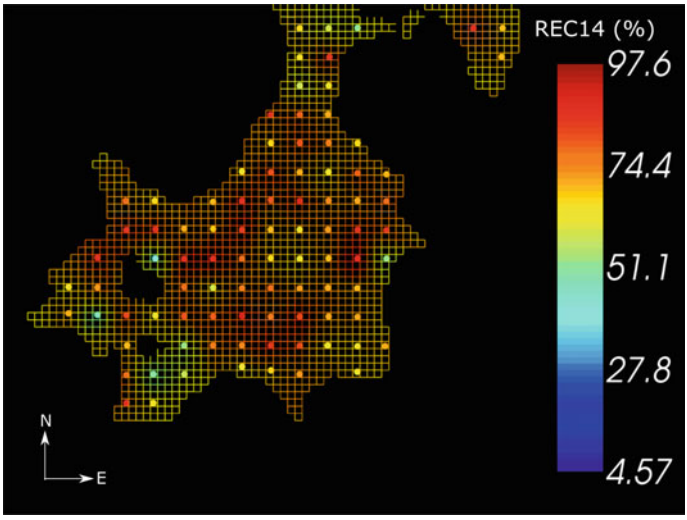


**Fig. 5.6** Block model with the samples

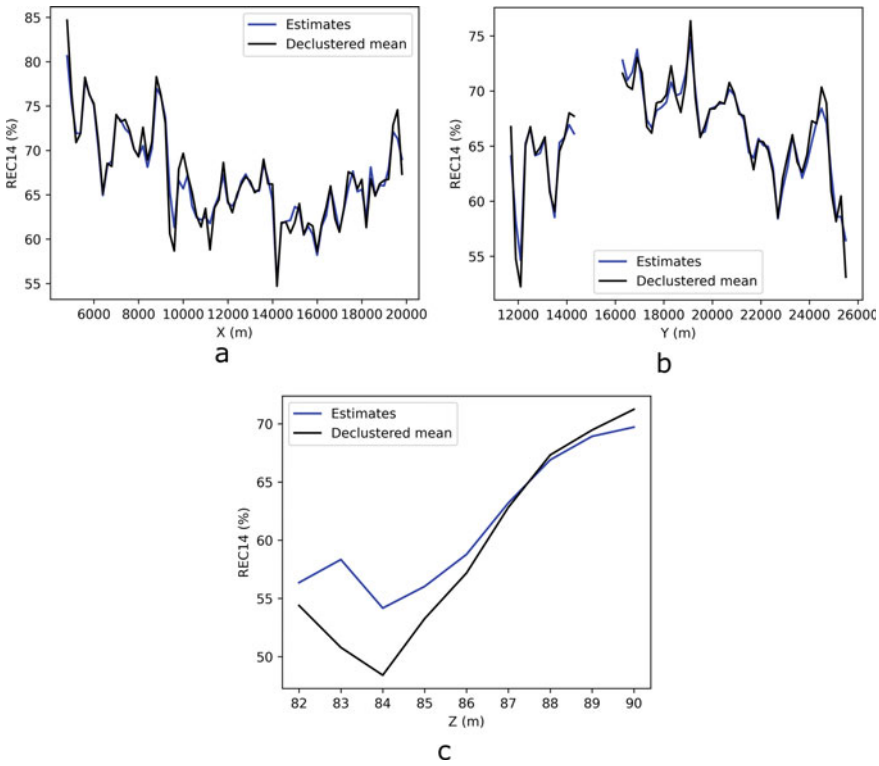


**Fig. 5.7** Swath plot along with the **a** $X$, **b** $Y$, and **c** $Z$ directions

areas of higher elevations. This lack of data in the areas of lower elevations resulted in discrepancies in the swath plot.

### *5.5.2 Comparison with Kriging Using Point Covariances*

Table 5.1 shows the cross-validation results for kriging with samples of different support and kriging using point covariances. The estimates obtained by kriging with samples of different are more accurate, as the mean error is closer to zero. Moreover, kriging with samples of different support resulted in higher precision. For this method, the standard deviation of the error, the mean absolute error, and the mean squared error are lower. The mean squared error obtained by kriging with samples of different support is 4.5% lower than the mean squared error obtained by kriging using point covariances.

The results emphasize the capacity of kriging to handle samples of different support. Practitioners often overlook that the kriging system may handle data of

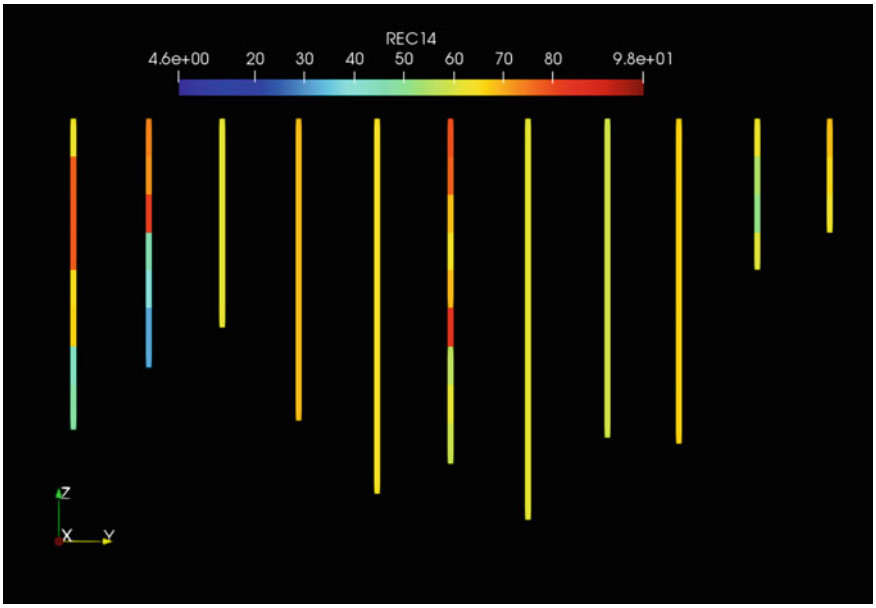


**Fig. 5.8** Cross section of the drill holes with stratigraphic coordinates. The vertical exaggeration is 20:1

**Table 5.1** Comparative table between kriging with samples of different support and kriging using point covariances

| | Kriging with samples of different support (using average covariances) | Kriging using point covariances |
|---|---|---|
| Count | 2342 | 2342 |
| Mean error (%) | 0.29 | 0.45 |
| Std. Dev. of the error (%) | 9.48 | 9.69 |
| Mean absolute error (%) | 7.06 | 7.32 |
| Mean squared error ($\%^2$) | 89.97 | 94.02 |

different support (Journel 1986). In the example, kriging was used to estimate grades in a mineral deposit using samples with different lengths.

In comparison against kriging using point covariances, kriging with samples of different support produced more accurate and precise estimates. When the samples have different supports, this difference should be considered in the kriging system through average covariances.

## References

Bassani MAA, Coimbra Leite Costa JF (2016) Grade estimation with samples of different length. Appl Earth Sci 125(4):202–207

Deutsch CV (2002) Geostatistical reservoir modeling. Oxford University Press, New York

Isaaks HE, Srivastava MR (1989) An introduction to applied geostatistics. Oxford University Press, Oxford

Journel AG (1986) Geostatistics: models and tools for the earth sciences. Math Geol 18(1):119–140

Pyrcz MJ, Deutsch CV (2014) Geoestatistical reservoir modeling. Oxford University Press, New York

Rubio RH, Koppe VC, Costa JFCL, Cherchenevski PK (2015) How the use of stratigraphic coordinates improves grade estimation. Rem: Revista Escola de Minas 68(4):471–477

# Chapter 6
# Case Study of Direct Sequential Simulation with Data of Different Support


The majority of the theory about using data of different support has already been covered in the previous chapters. This chapter shows a case study of Direct Sequential Simulation (DSS) to integrate data of different support in a mining context. The result is a series of equally probable grade models that may be directly applied for stochastic mine planning. Also, these grade models provide a measure of uncertainty. The chapter highlights some practical aspects of DSS with data of different support. Moreover, the impact of the data support on uncertainty is discussed.

## 6.1 Dataset Presentation

The dataset used is the same as in Chap. 5, which shows a thorough exploratory data analysis. In this chapter, we emphasize the dataset's main characteristics used for Direct Sequential Simulation. The dataset is obtained from a bauxite deposit, and the variable of interest is the proportion of coarse fragments, called REC14.

The dataset contains 686 drill holes. At 343 drill holes, the sample length is 0.5 m along the vertical direction (blue points in Fig. 6.1). The other 343 drill holes have one sample that spans the entire ore thickness (red points in Fig. 6.1). In this case, the sample grade is the average grade over the ore thickness. This situation mimics a mine operation whose sampling protocols changed along its lifetime.

Direct Sequential Simulation (DSS) requires a reference distribution at the support to be simulated (Soares 2001; Oz et al. 2003). The simulated values are drawn from the region of the reference distribution whose mean and variance match the simple kriging estimate and variance. Early attempts of DSS did not use the reference distribution (Caers 2000). However, the methods that sample from the reference distribution have shown better histogram reproduction (Soares 2001).

In this case, we are interested in creating high-resolution models, so the simulations are performed at point support. Although Sequential Simulation algorithms may be adapted to simulate grades directly at block support (Godoy 2003; Boucher



M. A. Arcari Bassani and J. F. Coimbra Leite Costa, *Geostatistics with Data of Different Support Applied to Mining Engineering*, Topics in Mining, Metallurgy and Materials Engineering, https://doi.org/10.1007/978-3-030-80193-9_6

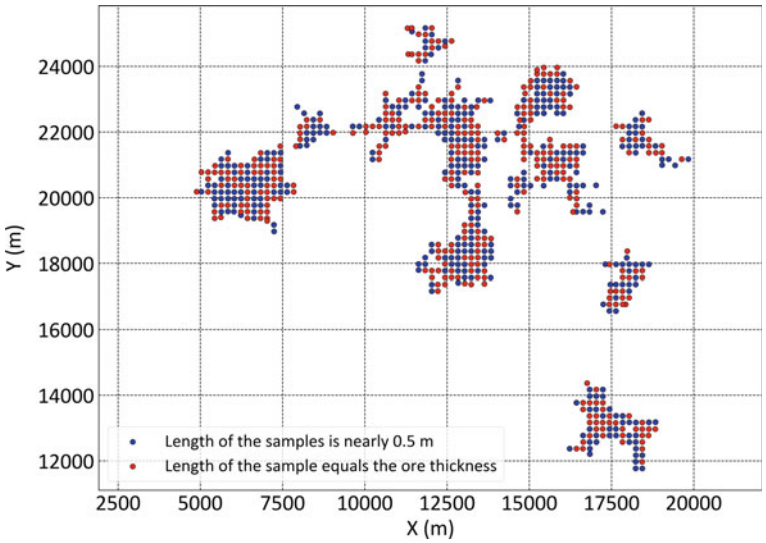


**Fig. 6.1** Location map of the samples

and Dimitrakopoulos 2009; Emery and Ortiz 2011), we preferred to use point-support simulation to add more flexibility. The point-support simulations may be block averaged according to any volume. This property is attractive when the mine planner wants to measure the grade uncertainty over an irregular volume. The simulated volume grade is the average of simulated-point values inside this volume (Journel and Huijbregts 1978). Another benefit of point simulation is that the grade models may be directly compared against the data. Block simulation usually requires changing the support of the histogram and variogram. This change of support diminishes the variance and smooths the extreme values, which may mask some valuable information.

Figure 6.2a shows the length-weighted histogram of the variable of interest considering all the samples. In contrast, Fig. 6.2b shows the histogram considering only the samples with nearly 0.5 m of length, called point-support histogram (the 0.5 m samples represent a "point" in the space as they are the shortest sampling interval). The standard deviation for the histogram considering only the point samples is higher, as expected. Also, the mean of the point-support histogram (Fig. 6.2b) is very similar to the mean of the mix-support histogram (Fig. 6.2a). This similarity indicates that the point-support samples are not preferentially sampled in either a high-grade or low-grade zone.

Cell declustering was performed to verify whether some clusters could affect the statistics of the point-support samples. In this context, Fig. 6.3 shows the QQ-plot between the equal-weighted and declustered histogram considering only the point samples. The QQ-plot shows that the two distributions are very similar, as the points follow the line $y = x$. This result shows that the equal-weighted histogram of REC14

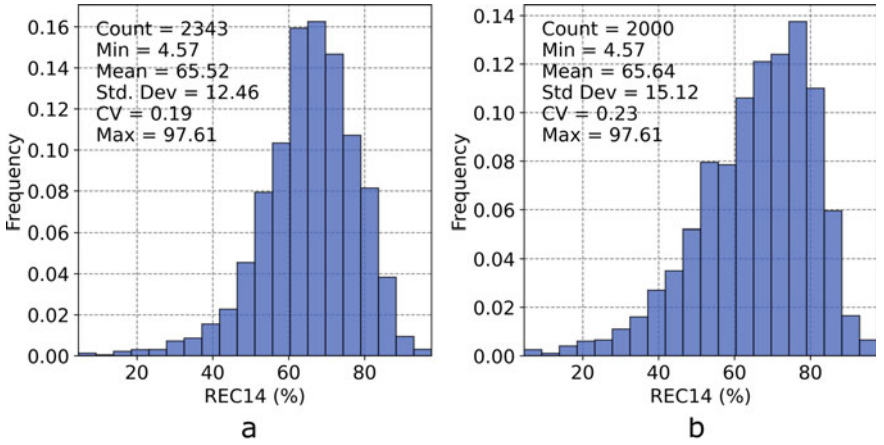


**Fig. 6.2** **a** Length-weighted histogram of REC14 considering all the samples and **b** equal-weighted histogram of REC14 considering only the point samples

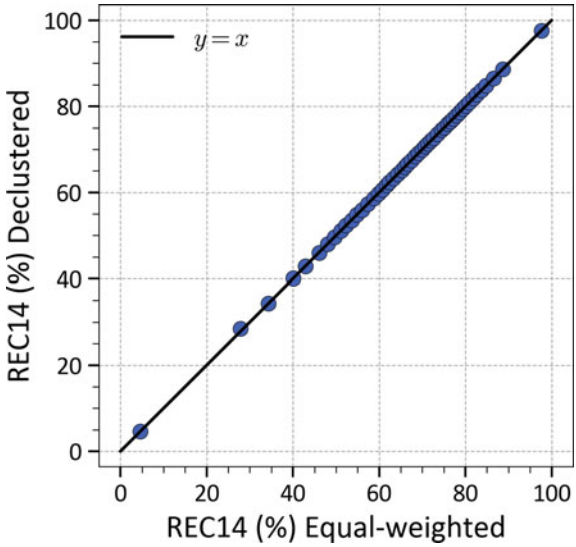


**Fig. 6.3** QQ-plot between the equal-weighted and declustered histogram of REC14 considering only the point samples

is representative of the area of interest. Thus, this histogram was used as a reference distribution for DSS.

This particular dataset has many point-support samples to obtain a point-support reference distribution (Fig. 6.2b). When the dataset exhibits a small number of point samples, the user may apply change-of-support techniques to obtain a point-support histogram. Several change-of-support methods are presented in the literature, such as the discrete Gaussian model (Journel and Huijbregts 1978), Affine (Isaaks and Srivastava 1989), and indirect lognormal (Isaaks and Srivastava 1989).

## 6.2 Spatial Continuity Analysis

Similar to the histogram, Direct Sequential Simulation (DSS) also requires a variogram model at the support to be simulated, that is, point support. The variogram model was obtained by variogram deconvolution and is the same variogram model used in Chap. 5. One advantage of the DSS over the Gaussian simulation methods is that kriging is performed in the space of original units. As a result, the variogram model used for DSS is the variogram model of the original variable. The Gaussian simulation methods require that the original data are transformed into Gaussian values. The variogram model is then fitted to these Gaussian values.

Figure 6.4 shows the point-support variogram model. The experimental variogram was calculated using all the available data and is called a block experimental variogram. The block variogram is obtained by variogram upscaling of the point-support variogram model (Eq. 4.6 in Chap. 4). Fitting the block variogram to the experimental variogram is not straightforward and required some trial and error. Increasing the nugget effect of the point-support variogram elevates the point-support variogram line. However, a higher nugget effect increases the variogram within blocks, which decreases the block variogram. This result occurs because the block variogram is the variogram between blocks minus the variogram within blocks (see Chap. 4, Eqs. 4.6–4.8).

The direction of major spatial continuity is horizontal and agrees with the sedimentary process that formed the deposit. The direction of minor spatial continuity is vertical. This spatial continuity pattern is widely observed at sedimentary formations such as coal deposits and oil reservoirs. Equation 6.1 shows the variogram model. The variogram is standardized so that the sill equals one. The standardized variogram model is used during DSS to define the sample the global histogram using the Soares approach (see Chap. 3).

$$\begin{aligned}\gamma(\mathbf{h}) = 0.11 &+ 0.59 \cdot \mathrm{Sph}\left(\frac{\mathrm{NS}}{300\,\mathrm{m}}, \frac{\mathrm{EW}}{300\,\mathrm{m}}, \frac{\mathrm{vert.}}{3\,\mathrm{m}}\right) \\ &+ 0.30 \cdot \mathrm{Sph}\left(\frac{\mathrm{NS}}{5000\,\mathrm{m}}, \frac{\mathrm{EW}}{5000\,\mathrm{m}}, \frac{\mathrm{vert.}}{7\,\mathrm{m}}\right)\end{aligned} \tag{6.1}$$

The geostatistical simulations are more sensitive to the variogram model than kriging estimates. In this context, we presented a more detailed variogram discussion here than in Chap. 5, which covers kriging estimates.

## 6.3 Geostatistical Simulations

The simulations were performed using Direct Sequential Simulation (DSS) with data of different support, which is known as Block Sequential Simulation—BSSIM (Liu and Journel 2009). The variable of interest is simulated on a high-resolution grid.

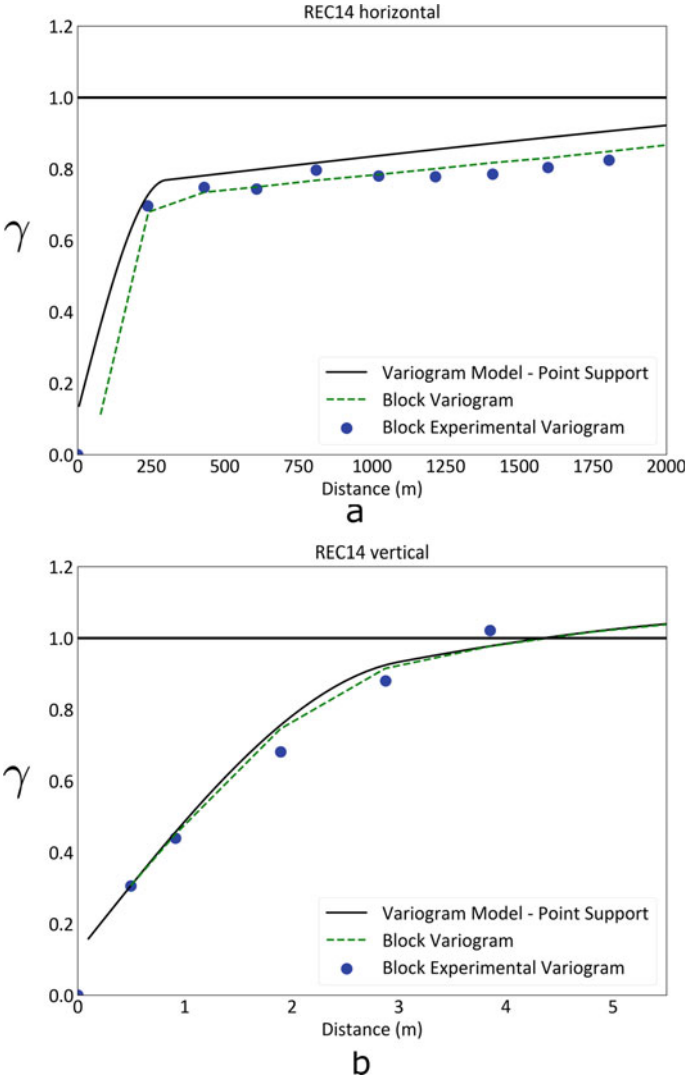


**Fig. 6.4** Experimental variogram, variogram model at point support, and block variogram along with the **a** horizontal and **b** vertical directions

The grid spacing is 12.5 m × 12.5 m × 0.5 m along the X, Y, and Z directions. The number of nodes along the X, Y, and Z directions is 1240, 1108, and 17, respectively. The entire grid was simulated, and then the simulated values outside the geological domain were clipped. In this case study, twenty-five realizations were built. The software for DSS consists of an executable that was published by Azevedo and Soares (2017). The sampling method for the local cumulative distributions is the Soares approach (Soares 2001).

The difference of support between the samples was considered in the kriging system through block-to-block covariances. The spacing between the discretization points is 0.50 m. For instance, a sample whose length is 1.5 m is represented by three discretization points. The discretization points are used to calculate the block-to-block and point-to-block covariances used in the kriging system.

## 6.4 Results and Discussion

### *6.4.1 Realizations*

Figure 6.5a, b shows two realizations obtained by DSS. Although both models are different, they have the same spatial characteristics. The high- and low-grade areas are in the same regions for both models. For comparison purposes, an estimated model was built with ordinary kriging (Fig. 6.5c). The estimated model shows a smoother transition between the grades due to the smoothing effect of kriging. On

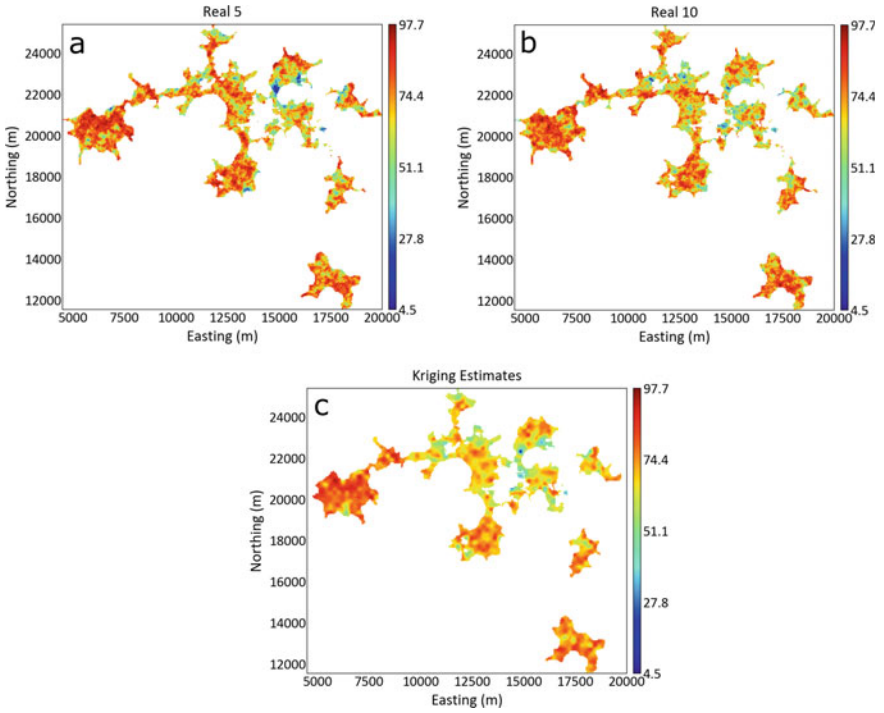


**Fig. 6.5** Maps of the **a** fifth and **b** fifteenth realizations, and **c** map of kriging estimates

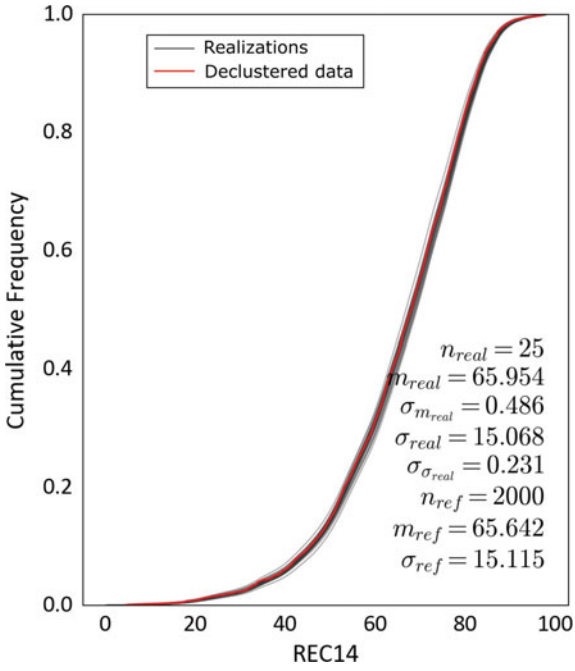


**Fig. 6.6** Histogram reproduction of the realizations

the other hand, the realizations show higher variability and characterize the deposit's true spatial variability.

### *6.4.2 Histogram Reproduction*

Figure 6.6 shows the histogram reproduction of the realizations. The histograms of the realizations are close to the histogram of the declustered data (see Fig. 6.6). This result shows that the realizations reproduced the distribution of the declustered data. Also, the histograms of the realizations are close to each other. This proximity indicates low global uncertainty. This result is expected as the area of interest is densely sampled.

### *6.4.3 Variogram Reproduction*

Figure 6.7 compares the experimental variogram of the realizations against the variogram model used to conditioning the realizations. The experimental variograms of the realizations were standardized so that the sill is one. The results show that the realizations reproduced the variogram model, as expected.

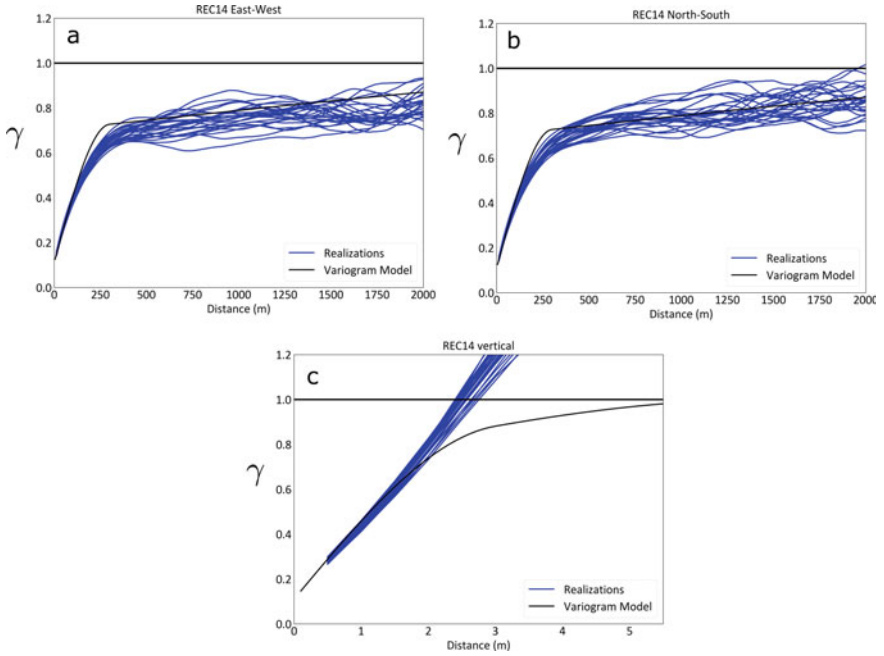


**Fig. 6.7** Variogram reproduction along the **a** East–West, **b** North–South, and **c** vertical directions

### *6.4.4 Post-processing*

Figure 6.8 shows the E-type of the realizations. The E-type consists of the average over all the realizations. As expected, the E-type shows a smooth map that resembles the kriging estimates (Fig. 6.5c).

Figure 6.9a shows the map of the standard deviation, which represents a measure of uncertainty. The standard deviation shows, for each grid node, the standard deviation over all the realizations. The regions where the standard deviation is low are the regions where all the realizations have similar simulated values. In other words, all the possible values are similar, and the practitioner knows reasonably well whether this region has either high or low grade (low uncertainty). In contrast, the regions with a high standard deviation mean the opposite: high uncertainty. As expected, the regions closer to the data points have lower uncertainty.

Figure 6.9b amplifies a region to demonstrate the effect of data support on uncertainty. Overall, the regions closer to the samples whose length is nearly 0.5 m have a lower standard deviation than the regions closer to the samples whose length corresponds to the ore thickness. This result agrees with the results shown by Horta et al. (2014) and is intuitive. For instance, a sample representing the average grade over 2 m contains less information than four aligned samples of 0.5 m. The four samples inform all the grades of the four 0.5 m intervals. In contrast, the 2 m sample does not inform if the grade at the first 0.5 m differs from that of the last 0.5 m. In this context,

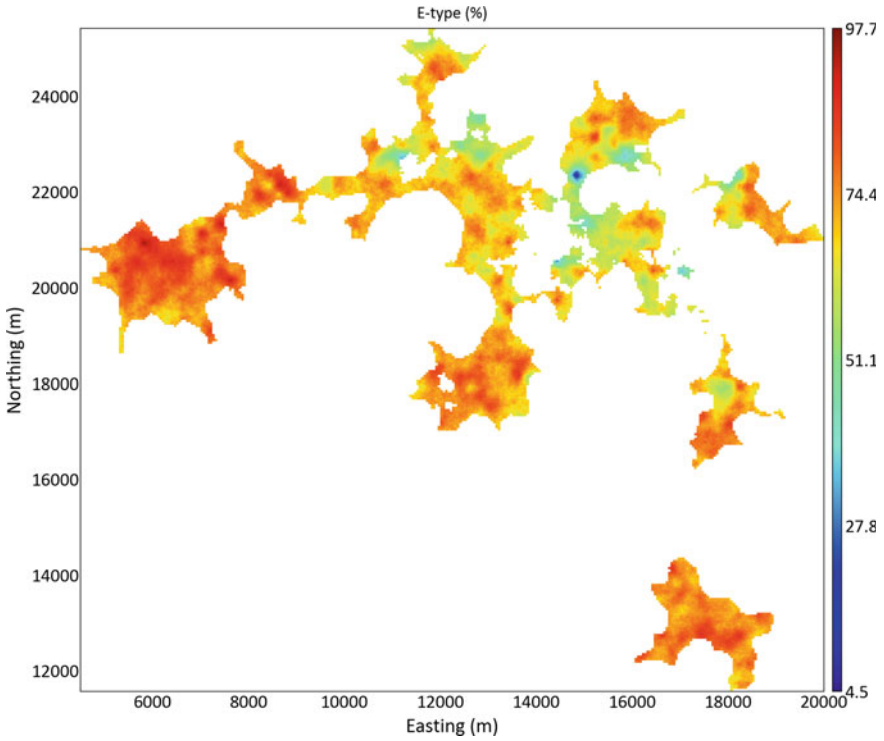


**Fig. 6.8** Map of the average over all the realizations (E-type)

Direct Sequential Simulation with samples of different support detected this loss of information, represented by the areas of higher uncertainty.

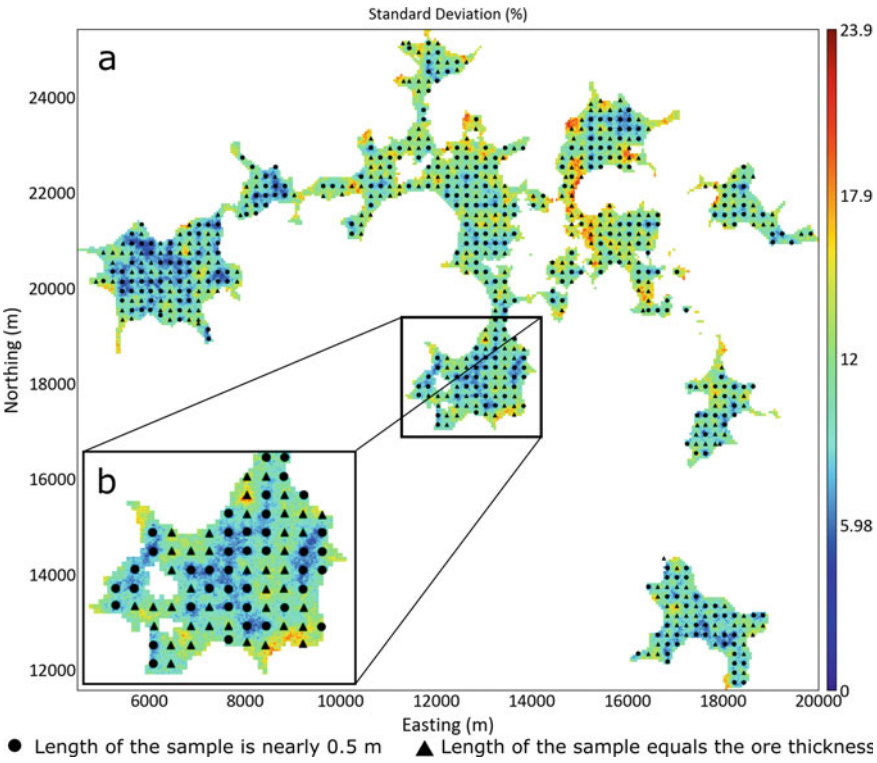


**Fig. 6.9** **a** Map of the standard deviation over all the realizations and **b** detailed view of a region of the deposit

## References

Azevedo L, Soares A (2017) Geostatistical methods for reservoir geophysics. Springer, Switzerland

Boucher A, Dimitrakopoulos R (2009) Block simulation of multiple correlated variables. Math Geosci 41(2):215–237

Caers J (2000) Adding local accuracy to direct sequential simulation. Math Geol 32(7):815–850

Emery X, Ortiz JM (2011) Two approaches to direct block-support conditional co-simulation. Comput Geosci 37(8):1015–1025

Godoy M (2003) The effective management of geological risk in long-term scheduling of open pit mines. PhD, University of Queensland

Horta A, Pereira MJ, Gonçalves M, Ramos T, Soares A (2014) Spatial modelling of soil hydraulic properties integrating different supports. J Hydrol 511:1–9

Isaaks E, Srivastava M (1989) An introduction to applied geostatistics. Oxford University Press, New York

Journel AG, Huijbregts CJ (1978) Mining geostatistics. Academic Press, New York

Liu Y, Journel AG (2009) A package for geostatistical integration of coarse and fine scale data. Comput Geosci 35(3):527–547

Oz B, Deutsch CV, Tran TT, Xie Y (2003) DSSIM-HR: a FORTRAN 90 program for direct sequential simulation with histogram reproduction. Comput Geosci 29(1):39–51

Soares A (2001) Direct sequential simulation and cosimulation. Math Geol 33(8):911–926

# Chapter 7
# Case Study of Sequential Indicator Simulation with Data of Different Support


This chapter illustrates the application of Sequential Indicator Simulation with data of different support to measure the geological complexity of a mineral deposit. We define the geological complexity based on the number of rock types and how connected they are in a mining operation. For example, an ore formation that contains a single rock type has minimum geological complexity. In contrast, an ore formation that contains five different rock types intermingled has high complexity.

Managing geological complexity is a crucial factor for the successful operation of mining activities. Consider, for instance, two rock types with two different processing routes. Mixing these rock types is likely to produce suboptimal results in terms of metallurgical recovery. The areas where these two rocks are in contact have high geological complexity. These areas may be prioritized for infill drilling so that their contacts become more accurate than they are currently.

This chapter shows how Sequential Indicator Simulation with data of different support may be applied to measure the geological complexity in an iron ore formation. The case study uses data derived from an iron ore deposit located in the Quadrilaterro Ferrifero region in Brazil.

## 7.1 Dataset Presentation

The dataset consists of diamond drill holes (DDH) with rock type information and the interpreted geological model. There are four rock types: (i) waste, (ii) hard itabirite, (iii) friable itabirite, and (iv) hematitite. These four rock types play different roles in the mining operation. Waste does not have economic value and is sent directly to the waste dump. The itabirites represent low-grade ore whose Fe contents range from 30 to 60% roughly. The hematitite has the highest Fe contents, exceeding 60%.

Figure 7.1 shows the drill hole samples and the interpreted geological model. The block size of the interpreted block model is 10 m $\times$ 10 m $\times$ 10 m along the $X$, $Y$, and $Z$ directions, respectively. The length of the drill hole samples is 10 m. The hematitite



M. A. Arcari Bassani and J. F. Coimbra Leite Costa, *Geostatistics with Data of Different Support Applied to Mining Engineering*, Topics in Mining, Metallurgy and Materials Engineering, https://doi.org/10.1007/978-3-030-80193-9_7

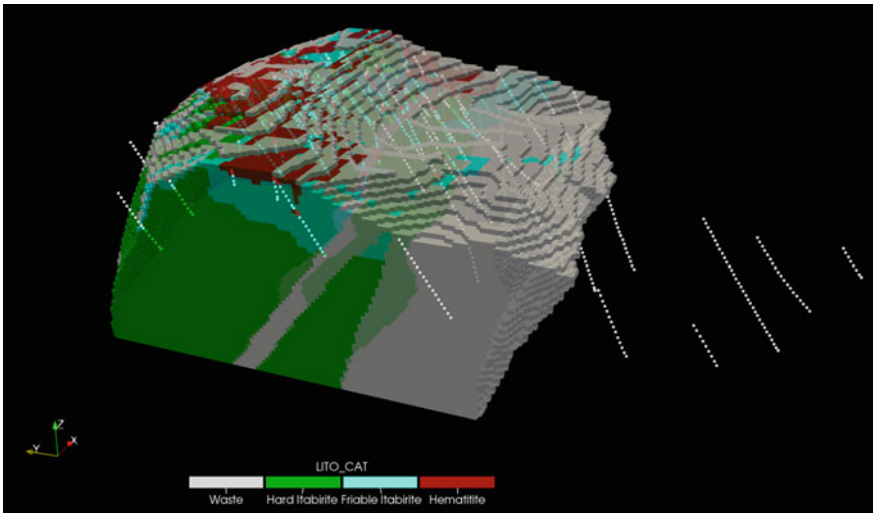


**Fig. 7.1** Drill hole samples and interpreted geological model. Note that the opacity of the interpreted geological model was reduced so that the drill holes are visible

and friable itabirite occur in the upper parts of the deposit in the form of lenses. In contrast, the hard itabirite and waste are more continuous and cover the majority of the deposit. Another interesting aspect is a waste dyke that crosses in the middle of the ore formation.

The interpreted geological model was built using interpreted cross sections (this method is also referred to as an explicit model). In this method, the geologist manually defines the contours of the mineralization in a series of cross sections or slices (Abzalov 2016; Sinclair and Blackwell 2002). Then the cross sections are linked together to create a wireframe or geological volume. Lastly, the block model is flagged according to the wireframes. Figure 7.2 shows a cross section of the interpreted block model together with the drill holes. Folding events caused the curvature of the deposit.

We selected four benches of the upper part of the deposit to measure its geological complexity. The upper part of the iron ore formation has four rock types intermingled, while the lower part consists of two very continuous rock types (hard itabirite and waste). Moreover, the upper part of the deposit contains the rock types with the highest Fe contents. Figure 7.3a shows the interpreted block model with low opacity with the selected benches highlighted. Figure 7.3b shows the selected benches of the interpreted block model and the drill hole samples inside the benches' volume.

Figure 7.4 shows plan views of the four benches. The four benches cover an area of $460 \times 530$ m$^2$ and have a total height of 40 m (10 m per bench). The areas where the rock type changes as the bench elevation decreases represent a challenge. Iron ore mining often uses large excavation equipment to enhance productivity. The drawback is that the drilling and blasting operations move large ore volumes and mix ore from two consecutive benches. If the rock types of the consecutive benches are

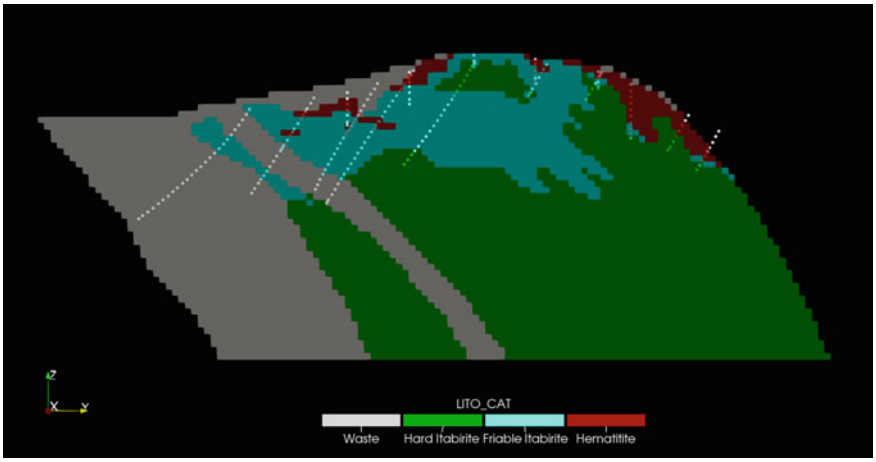


**Fig. 7.2** Vertical section of interpreted block model and drill hole samples. The opacity of the block model was reduced to improve the visibility of the drill hole samples

different, the blasted ore will consist of a mixture of these rock types. This mixture leads to suboptimal use of the processing plant. For instance, the Fe contents of the hematitite ore may be lowered due to the itabirites and waste mixture.

Figure 7.5 shows the global proportions of the rock types for the drill hole samples and the interpreted block model in the study area. The proportions of the interpreted block model are the reference proportions to be reproduced by the simulations. The highest proportion occurs for the itabirites, while hematitite has the lowest proportion.

## 7.2 Methodology

The proposed methodology combines the information from the interpreted block model and the drill hole samples. The primary assumption is that the rock type proportions of the interpreted block model at larger scales are well known, but the exact limits of the rock types at block scale are not. The drill hole samples represent information without error so that the simulations perfectly reproduce these samples.

The algorithm uses the larger-scale proportion of the interpreted block model and the drill hole samples to simulate the rock types. The result is a set of equally probable simulated models that honor both the large-scale proportions and drill hole samples.

The methodology consists of the following steps:

1. Calculate the average proportion of each rock type over a large scale;
2. Codification of the rock type variable into indicators;
3. Spatial continuity analysis of the indicators;
4. Sequential Indicator Simulation with data of different support;
5. Post-processing.

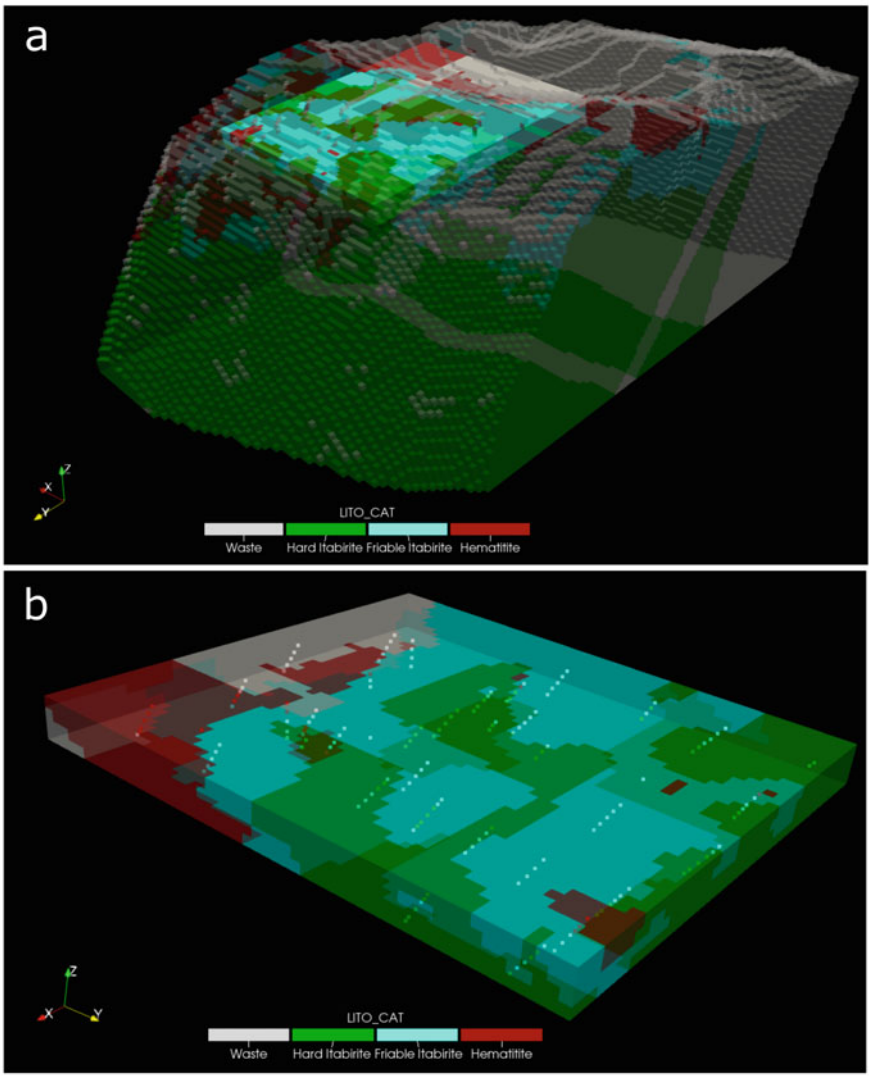


**Fig. 7.3** **a** Interpreted block model with low opacity with the four benches selected as the study area and **b** four benches selected as the study area and drill hole samples

## 7.3 Average Proportions and Indicators

The average proportion was calculated as the vertical proportion of each rock type over the four benches of study. The vertical proportions were obtained from the interpreted block model. If an interpreted block model is not available, one could replace it by calculating the moving window averages of the drill hole samples.

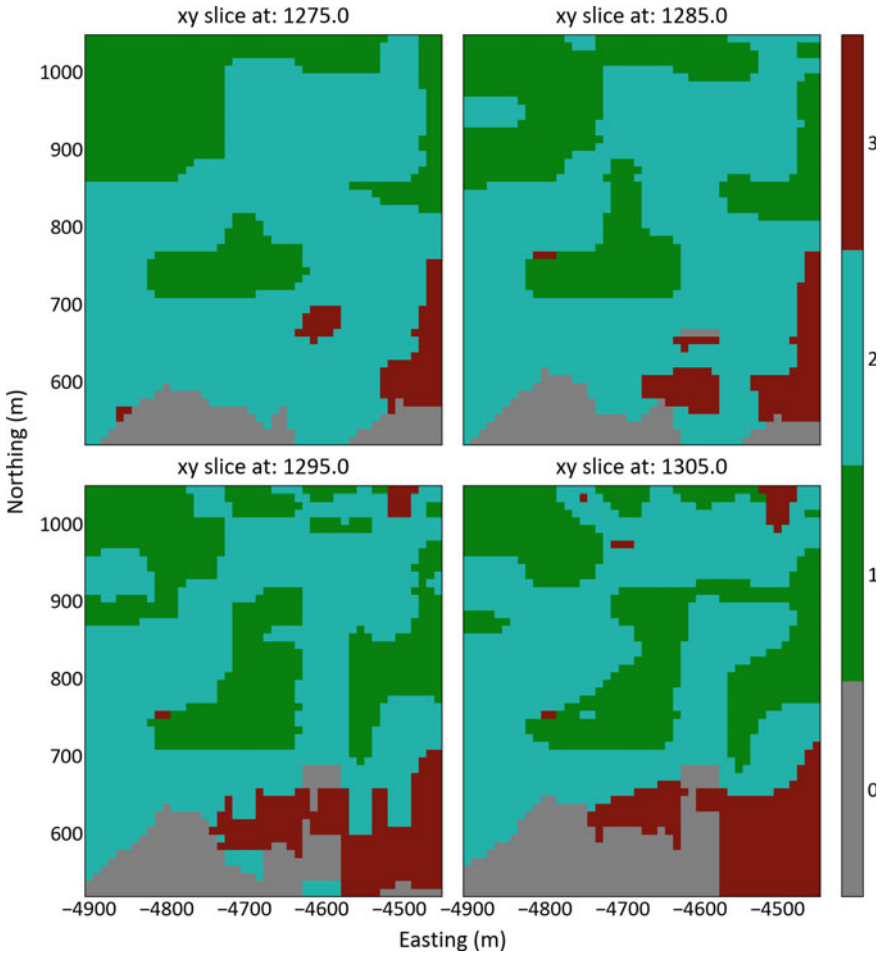


**Fig. 7.4** Horizontal slices of the four benches selected as the study area. In gray the waste, in dark green the hard itabirite, in light green the friable itabirite, and in red the hematitite

Figure 7.6 shows the vertical proportions of the four rock types. The regions where one single rock type is present at the four benches have a vertical proportion of one (this is the case for the hard itabirite in the northwestern corner of the study area).

The original dataset with rock type information was coded as indicators. The indicators for the rock types were obtained by Eq. 7.1:

$$i(\mathbf{u}_i; k) = \begin{cases} 1 \text{ if category } k \text{ prevails at location } \mathbf{u}_i \\ 0 \qquad\qquad\qquad \text{otherwise} \end{cases} \tag{7.1}$$

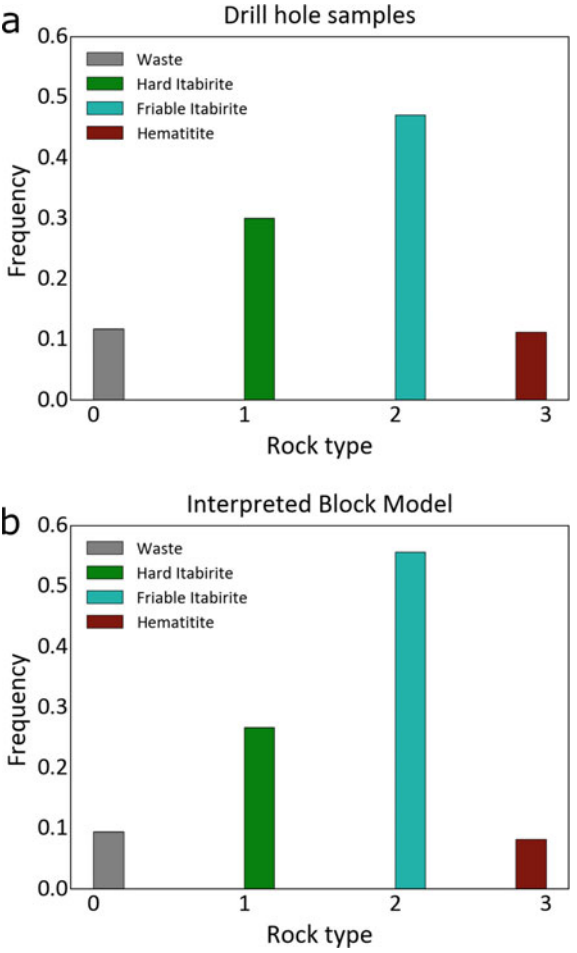


**Fig. 7.5** **a** Proportion of rock types in the drill hole samples and **b** the interpreted block model inside the study area

where $i(\mathbf{u}_i; k)$ is the indicator for category $k$ at the location $\mathbf{u}_i$. Figure 7.7 shows the original dataset with rock type information, while Fig. 7.8 the dataset coded as indicators for the four rock types.

## 7.4 Spatial Continuity Analysis

Figures 7.9, 7.10, 7.11 and 7.12 show the experimental indicator variograms and the variogram models for the main directions of anisotropy. The experimental variograms were calculated using all the drill hole samples. The experimental values were standardized so that the sill equals one.

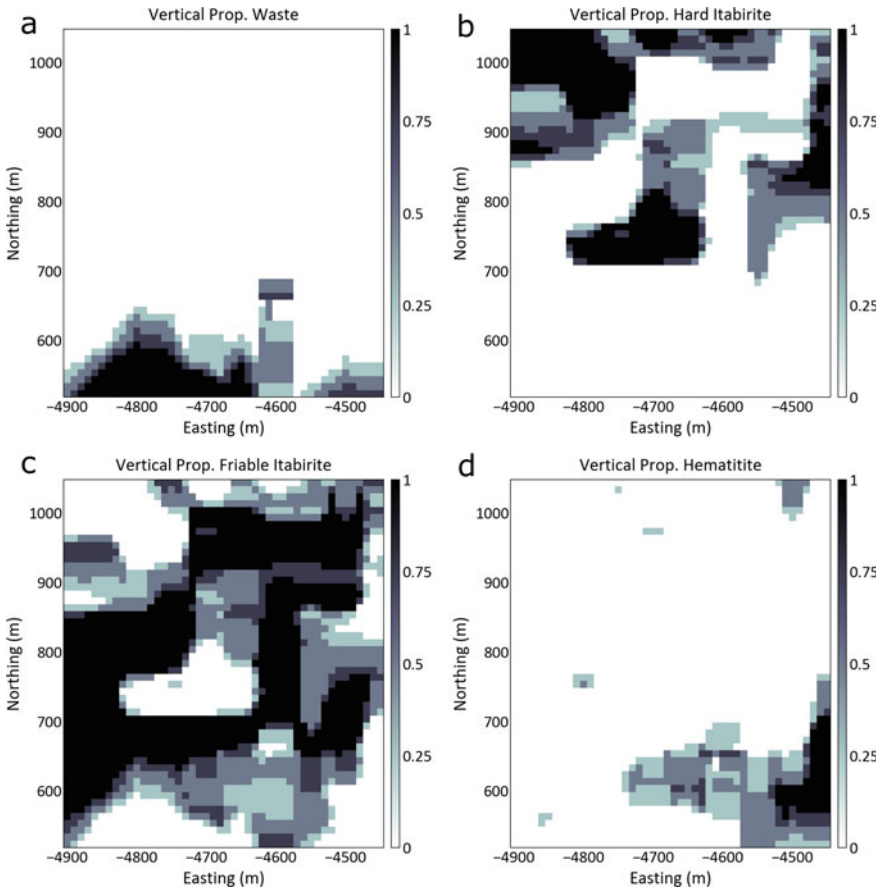


**Fig. 7.6** Average vertical proportions of **a** waste, **b** hard itabirite, **c** friable itabirite, and **d** hematitite obtained from the interpreted block model

The main directions of anisotropy found were NS/Dip 30°, N90°E, and N180°E/Dip 60°, which agree with the geological structures. The direction NS/Dip 30° aligns with the North Flank of the fold, which has a shallow dip. The direction N90°E follows the strike of the ore formation, which is the EW direction. The direction N180°E/Dip 60° is perpendicular to the other two main directions and is roughly the down-the-hole direction.

Table 7.1 describes the indicator variogram models of the four rock types. The nugget effect was set to 0.05 for all the cases. Although some experimental variograms exhibited a large short-scale variability, the nugget effect was kept small as rock types are usually continuous for small distances.

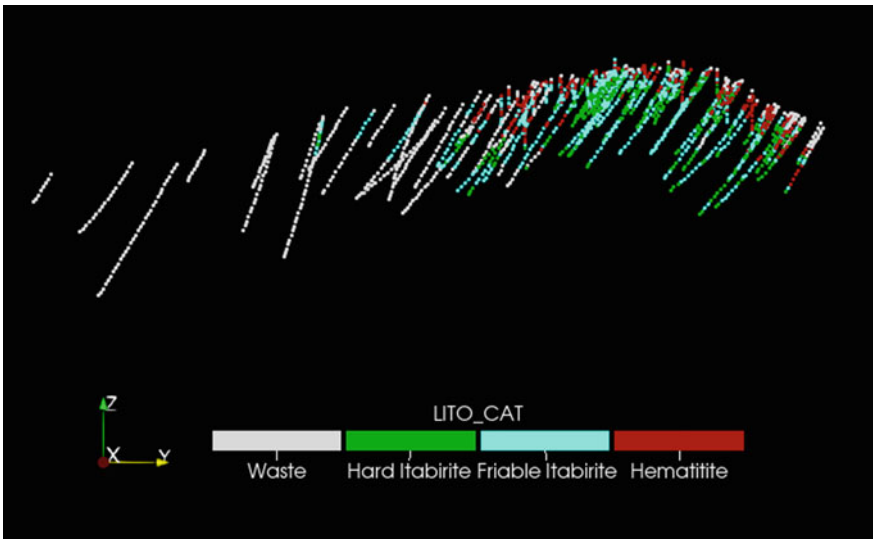


**Fig. 7.7** Drill hole samples colored by rock type

## 7.5 Geostatistical Simulations

The geostatistical simulations were performed with the software BlockSIS (Deutsch 2006). Fifty realizations were run. The conditioning information consisted of the drill hole samples and the vertical proportions of the rock types. Only the drill hole samples inside the study area were used to condition the simulations. Each indicator was kriged with its corresponding variogram model. This characteristic strength of the Sequential Indicator Simulation allows the geomodeler to inform different spatial continuities for different rock types.

The simulation grid corresponds to the four benches of the study area to avoid extrapolation. The grid size has 46 × 53 × 4 cells along the $X$, $Y$, and $Z$ directions while the cell size is 10 m × 10 m × 10 m, which mimics the resolution of the interpreted block model. A higher-resolution grid was not used as the drill hole samples have a nominal length of 10 m. Keeping the same vertical size of the grid cells and the drill hole samples avoids loss of information in sequential simulation algorithms (Rossi and Deutsch 2014).

The difference in support between the vertical proportions and the drill hole samples was considered by using block-to-block and point-to-block covariances in the indicator kriging system. In this case study, we assumed that the vertical proportions do not have errors and are considered hard data in the kriging system. Thus, the block kriging option was chosen in BlockSIS (Deutsch 2006). If the interpreted block model is considered uncertain (soft data), the correct approach is to choose the block cokriging option in BlockSIS.

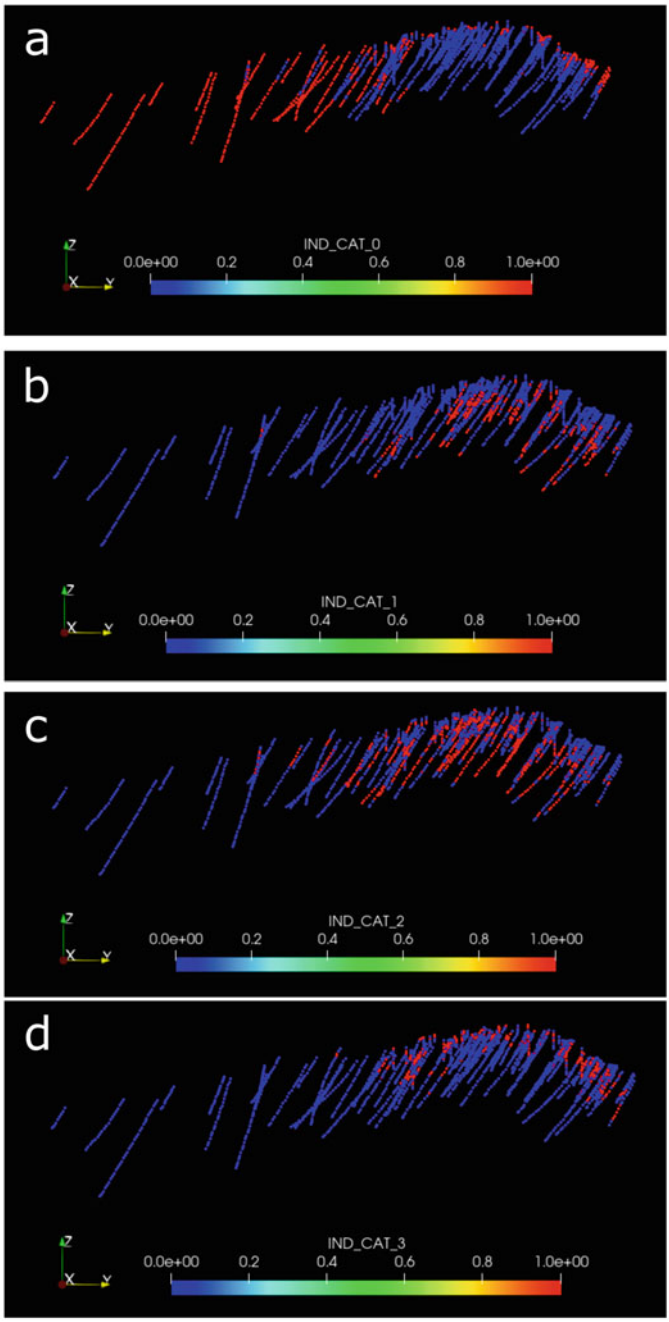


**Fig. 7.8** Drill hole samples colored by indicators of **a** waste, **b** hard itabirite, **c** friable itabirite, and **d** hematitite

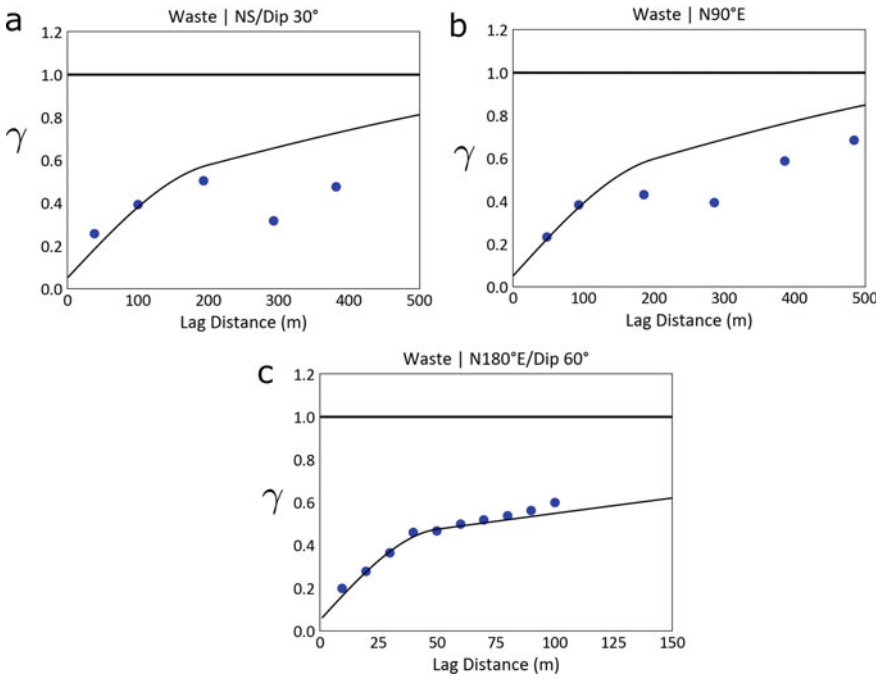


**Fig. 7.9** Experimental indicator variogram and variogram model of waste along with the directions of **a** major, **b** medium, and **c** minor spatial continuity

The block kriging option considers only the difference in support between the drill hole samples and the vertical proportions. In contrast, the block cokriging option considers the difference in both support and precision between the two types of data. In comparison to block cokriging, block kriging increases the weights assigned to the interpreted block model. Thus, the realizations are highly constrained by the vertical proportions and resemble the interpreted block model. On the other hand, the block cokriging option diminishes the influence of the vertical proportions on the realizations. In general, the realizations built by block kriging show less variability and uncertainty than the block cokriging counterparts. The decision of which kriging option to choose depends on the reliability of the interpreted block model. Moreover, a sensitivity analysis may be performed to check which option results in the more realistic model. These vertical proportions allow the geomodeler to use the interpreted block model as conditioning information. For instance, consider that a vertical proportion of hard itabirite over the four benches is 0.50. In this case, out of the four simulated blocks that comprise the four benches, only two simulated blocks are flagged as hard itabirite. In summary, the use of vertical proportions aids the simulation algorithm to create models that agree with the geologists' expertise portraited in the interpreted block model.

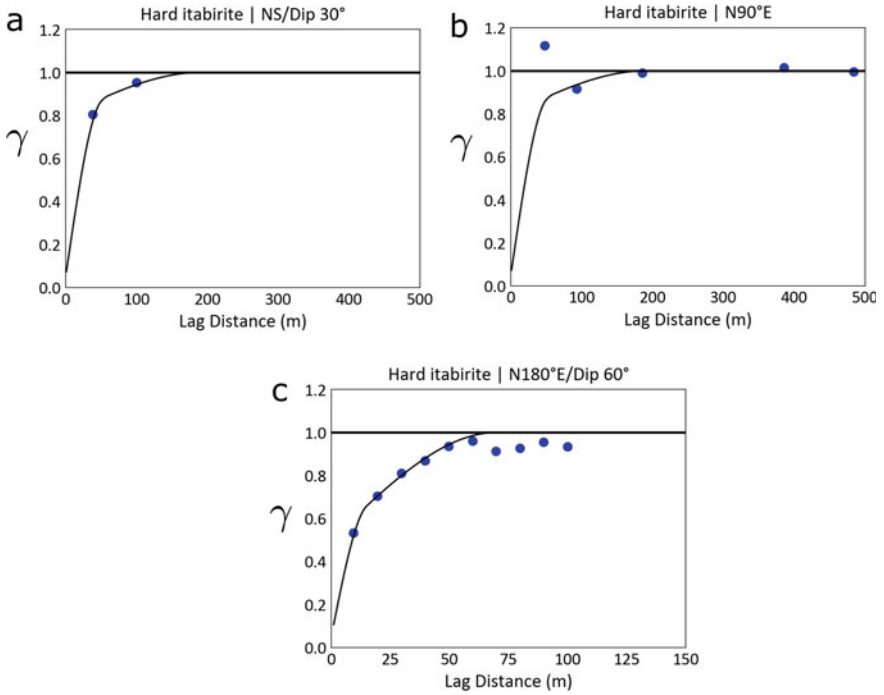


**Fig. 7.10** Experimental indicator variogram and variogram model of hard itabirite along with the directions of **a** major, **b** medium, and **c** minor spatial continuity

## 7.6 Results and Discussion

### *7.6.1 Realizations*

Figure 7.13 shows the interpreted block model and two realizations. The realizations have more variability than the interpreted block model, which is a smooth representation of reality. Moreover, the realizations are consistent with the interpreted block model. In other words, the regions where one particular rock type prevails in the interpreted block model are the same regions where this rock type prevails over all the realizations. For instance, the northwestern corner of the four benches has a high proportion of hard itabirite in the interpreted block model (see Fig. 7.13a). This high proportion of hard itabirite is present at the first and thirty-ninth realizations (Fig. 7.13b, c).

Figure 7.14 shows a scatter plot between the global rock type proportions of the interpreted block model against the global rock type proportions of the first realization. The results show that the rock type proportions were perfectly reproduced, as the points are close to the line $y = x$. The excellent reproduction of rock type proportions is an advantage of the Sequential Indicator Simulation with data

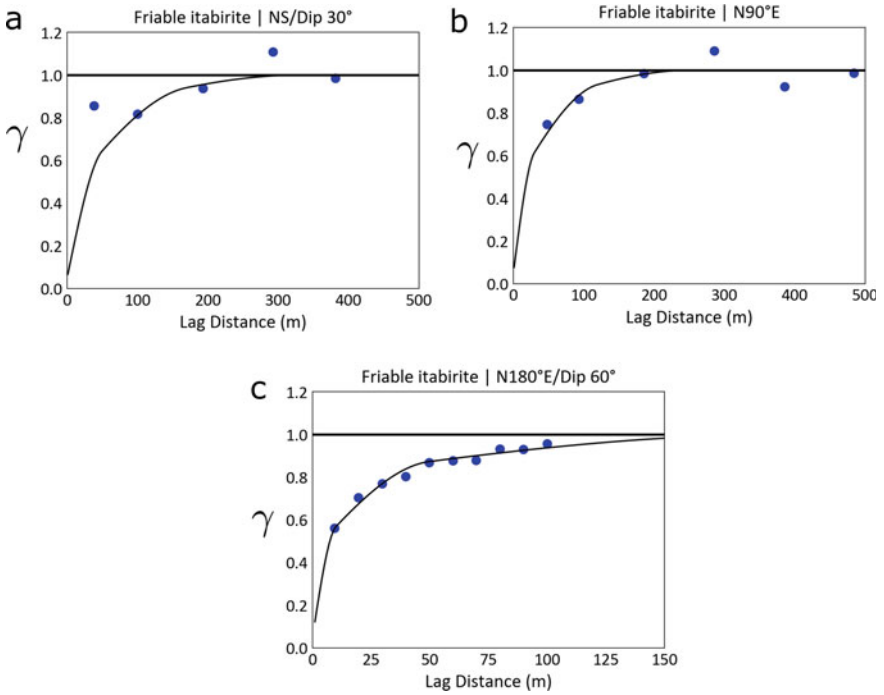


**Fig. 7.11** Experimental indicator variogram and variogram model of friable itabirite along with the directions of **a** major, **b** medium, and **c** minor spatial continuity

of different support compared to the conventional approach of Sequential Indicator Simulation, which uses only the drill hole samples. The conventional approach of Sequential Indicator Simulation often fails to reproduce the proportions of the rock types that represent a small fraction of the study volume (Soares 1998).

Figure 7.15 shows the vertical proportions of each rock type of the first realization. The vertical proportions of the first realization resemble the vertical proportions of the interpreted block model (Fig. 7.6).

### *7.6.2 Post-processing*

Figure 7.16 shows the probability of each category calculated over the fifty realizations, called E-type. For instance, consider a grid cell that is simulated as hematitite in twenty-five realizations out of the fifty. This particular grid cell has a 0.50 probability of being hematitite. In summary, the E-type model informs, for any grid cell, the probability that a specific rock type prevails in this cell. The E-type model agrees with the interpreted block model (Fig. 7.3b). For instance, the

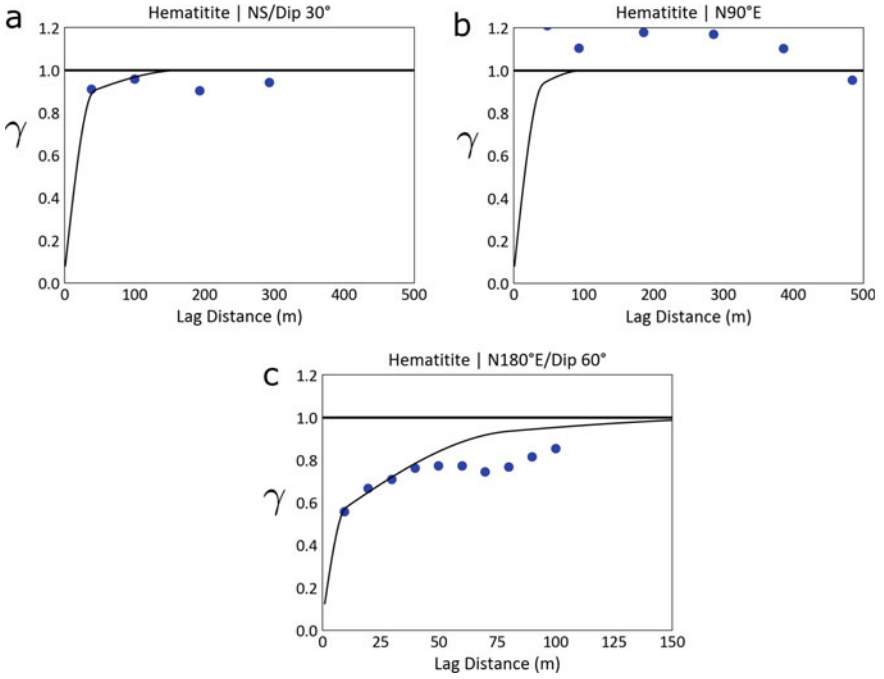


**Fig. 7.12** Experimental indicator variogram and variogram model of hematitite along with the directions of **a** major, **b** medium, and **c** minor spatial continuity

highest probabilities of being waste occur in the same regions where the waste is the dominant rock type (considering its close vicinity) in the interpreted block model.

Figure 7.17 shows the uncertainty, calculated as one minus the highest probability (Goovaerts 1997). The highest probability is informed by the E-type model (Fig. 7.16). A region where a particular rock type is dominant has little uncertainty. For instance, the probability of being hard itabirite in the northwestern region of the model is roughly one (see Fig. 7.16b). In other words, there is no question that this region is hard itabirite, so its uncertainty is zero (Fig. 7.17). The highest uncertainty occurs when the four rock types have the same probability of 0.25, which results in an uncertainty of 0.75. The uncertainty model shows that the highest uncertainties occur around the contact between rock types, as expected. These results are consistent with those found by Boucher et al. (2014) and Carvalho et al. (2014).

From a practical perspective, the uncertainty model informs the geological complexity of the deposit. The geological complex areas are the areas near the contacts and present two challenges for the mining operation: (i) the contacts are uncertain, and (ii) the risk of dilution and ore loss is exacerbated. The correct destination of a block depends on its rock type. When the rock type of a particular block is uncertain, choosing the correct processing route for this block is difficult. Moreover, these geological complex areas are prone to dilution and ore loss. The

**Table 7.1** Indicator variogram models for the four rock types

| Rock type | Structure | Contribution | Range NS/Dip 30° (m) | Range N90°E (m) | Range N180°E/Dip 60° (m) |
|---|---|---|---|---|---|
| Waste | Nugget Effect | 0.05 | 0 | 0 | 0 |
| | Spherical | 0.35 | 200 | 200 | 50 |
| | Spherical | 0.60 | 1000 | 900 | 600 |
| Hard itabirite | Nugget Effect | 0.05 | 0 | 0 | 0 |
| | Spherical | 0.45 | 50 | 50 | 15 |
| | Spherical | 0.30 | 60 | 60 | 70 |
| | Spherical | 0.20 | 190 | 190 | 70 |
| Friable itabirite | Nugget Effect | 0.05 | 0 | 0 | 0 |
| | Spherical | 0.40 | 50 | 30 | 10 |
| | Spherical | 0.35 | 170 | 120 | 50 |
| | Spherical | 0.20 | 330 | 250 | 200 |
| Hematitite | Nugget Effect | 0.05 | 0 | 0 | 0 |
| | Spherical | 0.45 | 40 | 40 | 10 |
| | Spherical | 0.35 | 45 | 45 | 80 |
| | Spherical | 0.15 | 170 | 100 | 200 |

blasting operations and equipment excavation are unable to extract the geological volumes near the contacts perfectly. The result is waste mixed with ore (dilution) and ore that is not extracted (ore loss).

The correct identification of the complex geological areas allows the mine planning team to take the required actions to mitigate these effects. For instance, these areas may be prioritized for infill drilling so that their uncertainty is reduced. Another action is to use high-selectivity equipment to mine these complex geological areas to avoid dilution and ore loss.

Further use of the geological uncertainty model involves mineral resources classification. The geological uncertainty may be considered when the mineral resources are classified as measured (low uncertainty), indicated (medium uncertainty), and inferred (high uncertainty). In this case, the regions with high geological uncertainty would be classified as inferred, with medium uncertainty as indicated, and with low uncertainty as measured.

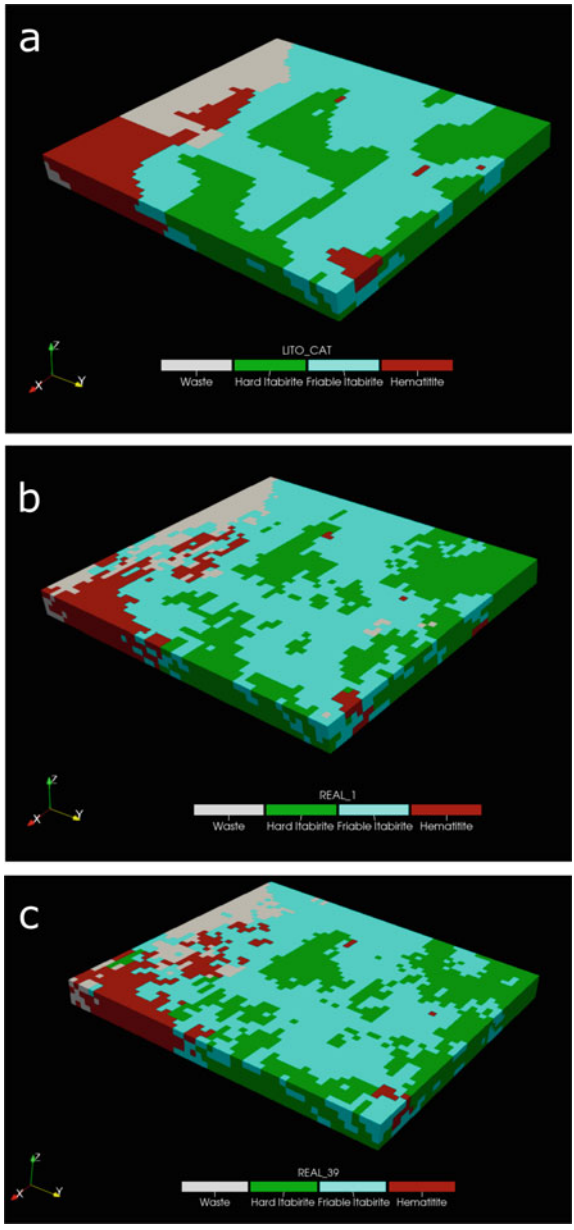


**Fig. 7.13** **a** interpreted block model, **b** first realization, and **c** thirty-ninth realization

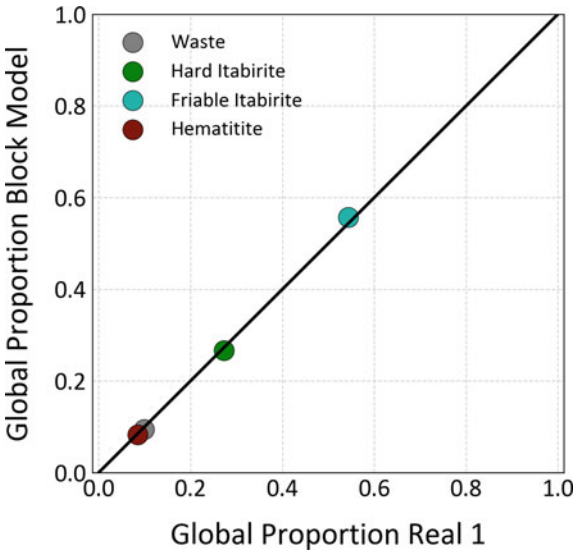


**Fig. 7.14** Global proportion of rock types for the interpreted block model and first realization

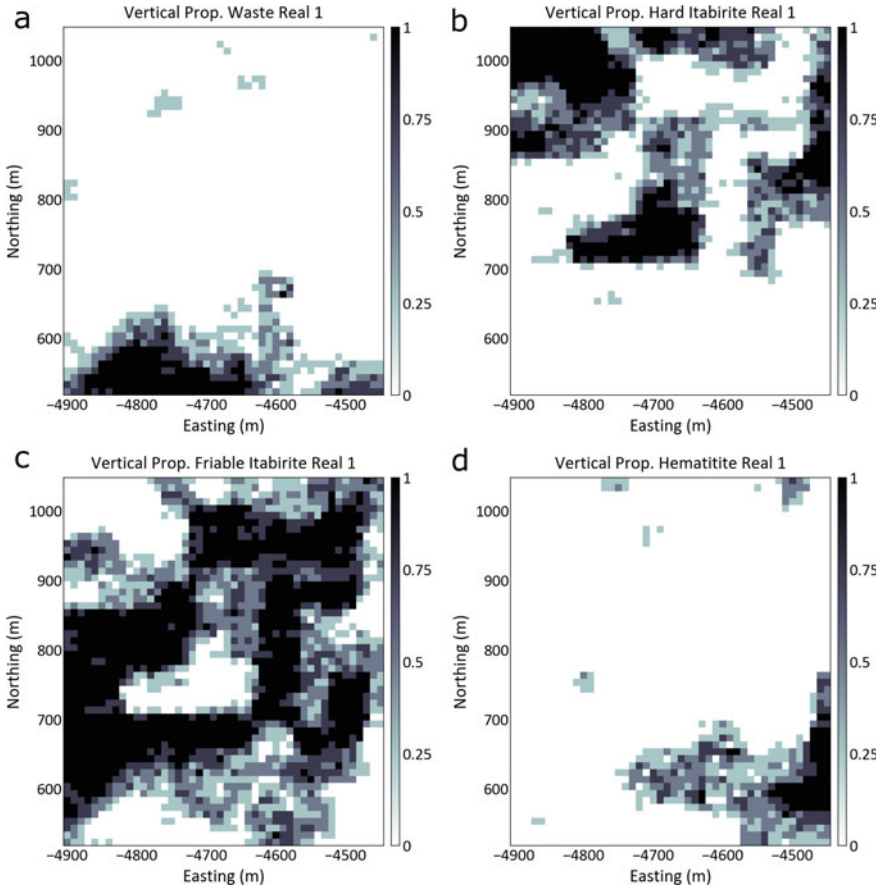


**Fig. 7.15** Average vertical proportions of **a** waste, **b** hard itabirite, **c** friable itabirite, and **d** hematitite of the first realization

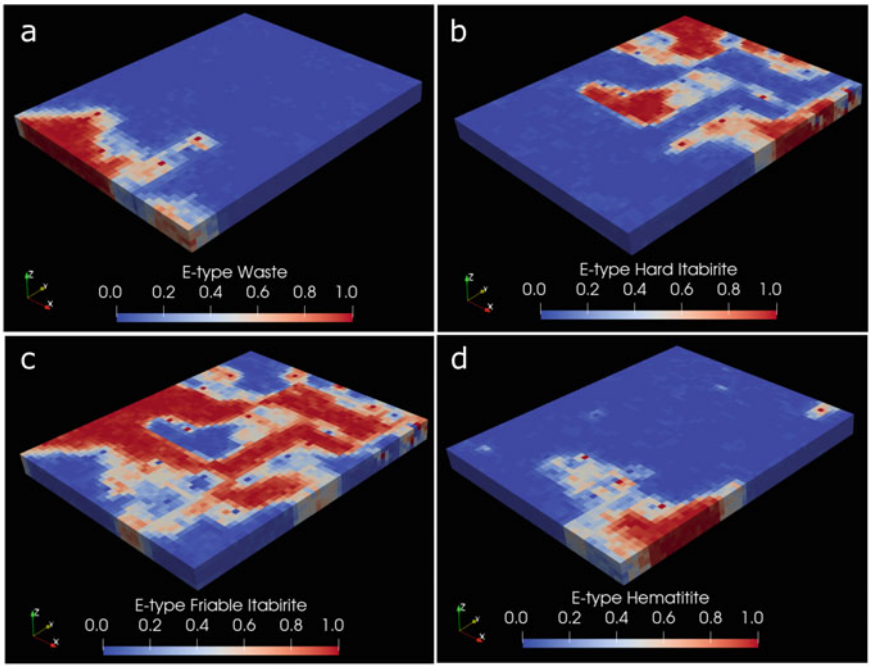


**Fig. 7.16** E-type of **a** waste, **b** hard itabirite, **c** friable itabirite, and **d** hematitite

**Fig. 7.17** Uncertainty model

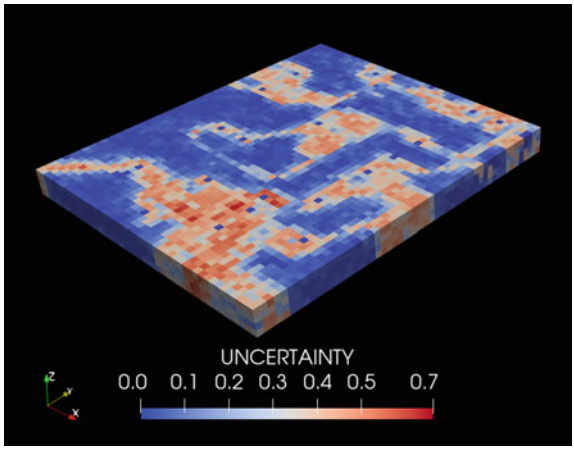


## References

Abzalov M (2016) Applied mining geology, vol 12. Springer International Publishing, Switzlerand

Boucher A, Costa JF, Rasera LG, Motta E (2014) Simulation of geological contacts from interpreted geological model using multiple-point statistics. Math Geosci 46(5):561–572

Carvalho J, Correia P, Menezes S, Peixoto C, Soares A (2014) Uncertainty assessment of the orebodies geometry by using block indicator simulation. Mathematics of planet earth. Springer, Berlin, pp 731–734

Goovaerts P (1997) Geostatistics for natural resource evaluation. Oxford University Press, Oxford

Deutsch CV (2006) A sequential indicator simulation program for categorical variables with point and block data: BlockSIS. Comput Geosci 32(10):1669–1681

Rossi ME, Deutsch CV (2014) Mineral resource estimation. Springer, Berlin

Sinclair AJ, Blackwell GH (2006) Applied mineral inventory estimation. Cambridge University Press, London

Soares A (1998) Sequential indicator simulation with correction for local probabilities. Math Geol 30(6):761–765

# Chapter 8
# Conclusions


Geostatistics provides an extensive toolbox to build grade models required for mining planning. This extensive toolbox often is not fully explored, and practitioners tend to use the more traditional algorithms such as ordinary kriging. The result is those geostatistical algorithms that allow the integration of data of different support are disregarded.

In this book, we emphasize the importance of using the data as they are. In other words, if two types of data have different support, this difference must be considered. Most importantly, Chapter 2 allows the practitioner to understand when the difference of support impacts more or less the estimates based on the variogram model.

We also tried to improve the clarity of this topic by focusing on practical applications. The use of data of different support in Geostatistics is usually taught in Geostatistics courses for graduate students. However, the classroom environment typically uses simplified examples. The primary goal is to facilitate the students' understanding of the fundamentals. In this book, we show case studies with data obtained from real mineral deposits.

The case studies covered the major applications of grade models used in Mining Engineering. Chapter 5 shows an application of grade estimation using ordinary kriging with data of different support. Ordinary kriging is the main interpolation engine for mineral resources estimation. Chapter 6 shows the application of Direct Sequential Simulation to measure grade uncertainty when the data have different support. Geostatistical Simulation builds equally probable models that are used for stochastic mine planning. In addition, the simulated models provide a measure of uncertainty. Chapter 7 applies the Sequential Indicator Simulation with data of different support to measure the geological uncertainty. Often, the geological uncertainty is the highest uncertainty present in a mineral resources model. The technique presented in Chapter 7 integrates the information provided by the interpreted block model and the drill hole samples for categorical variables. The interpreted block model represents the mine geologists' expertise.



M. A. Arcari Bassani and J. F. Coimbra Leite Costa, *Geostatistics with Data of Different Support Applied to Mining Engineering*, Topics in Mining, Metallurgy and Materials Engineering, https://doi.org/10.1007/978-3-030-80193-9_8